DOT/FAA/RD/PS-88/11

Project Report
ATC-160

Observability of Microbursts with Doppler Weather Radar During 1986 in Huntsville, AL

D. A. Clark

29 December 1988

Lincoln Laboratory
MASSACHUSETTS INSTITUTE OF TECHNOLOGY
LEXINGTON, MASSACHUSETTS

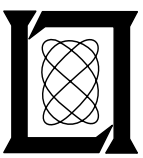

Prepared for the Federal Aviation Administration,
Washington, D.C. 20591

TECHNICAL REPORT STANDARD TITLE PAGE

1. Report No.	2. Government Accession No.	3. Recipient's Catalog No.
DOT/FAA/RD/PS-88/11		

4. Title and Subtitle	5. Report Date
Observability of Microbursts with Doppler Weather Radar During 1986 in Huntsville, AL	29 December 1988
	6. Performing Organization Code

7. Author(s)	8. Performing Organization Report No.
David A. Clark	ATC-160

9. Performing Organization Name and Address	10. Work Unit No. (TRAIS)
Lincoln Laboratory, MIT P.O. Box 73 Lexington, MA 02173-0073	11. Contract or Grant No. DTFA-01L-83-4-10579
	13. Type of Report and Period Covered
12. Sponsoring Agency Name and Address Department of Transportation Federal Aviation Administration 800 Independence Avenue, SW Washington, DC 20591	Project Report
	14. Sponsoring Agency Code

15. Supplementary Notes

The work reported in this document was performed at Lincoln Laboratory, a center for research operated by Massachusetts Institute of Technology under Air Force Contract F19628-85-C-0002.

16. Abstract

This report investigates the observability of low-level wind shear events using Doppler weather radar through a comparison of radar and surface wind sensor data. The data was collected during 1986 in the Huntsville, AL area as part of the FAA Terminal Doppler Weather Radar (TDWR) development program. Radar data were collected by both an S-band radar (FL-2) and C-band radar (UND). Surface data were collected by a network of 77 weather sensors covering an area of nearly 1000 square km centered approximately 15 km to the northwest of the FL-2 radar site. The UND site was located at the approximate center of the surface sensor network

A list of 131 microbursts which impacted the surface sensor network is presented. Particular emphasis is on the 107 events for which both radar data and surface data were available. Of these events, 14 were not observed by the surface network, while two events were not identified as microbursts by radar. Possible explanations of these missed microburst identifications are presented. The first case was an instance of the radar viewing a weak, asymmetric event from an unfavorble viewing angle. The second case describes an extremely shallow microburst outflow occurring at a height too low to be observed by the lowest elevation scan of the radar. In each of these cases, the featured microburst was very weak and, although a microburst-strength differential velocity was not observable by radar, in both instances the divergent wind pattern associated with the event was clearly evident in the radar velocity data field. All microbursts which exhibited a differential velocity of in excess of 13 m/s were identified by radar. No microbursts went unobserved as the result of insufficient signal return.

17. Key Words		18. Distribution Statement
Terminal Doppler Weather Radar	observability	Document is available to the public through the National Technical Information Service, Springfield, VA 22161.
wind shear	mesonet	
microburst	velocity couplet	
divergent outflow winds	differential velocity	

19. Security Classif. (of this report)	20. Security Classif. (of this page)	21. No. of Pages	22. Price
Unclassified	Unclassified	59	

FORM DOT F 1700.7 (8-69)

ABSTRACT

This report investigates the observability of low-level wind shear events using Doppler weather radar through a comparison of radar and surface wind sensor data. The data were collected during 1986 in the Huntsville, AL area as part of the FAA Terminal Doppler Weather Radar (TDWR) development program. Radar data were collected by both an S-band radar (FL-2) and C-band radar (UND). Surface data were collected by a network of 77 weather sensors covering an area of nearly 1000 square km centered approximately 15 km to the northwest of the FL-2 radar site. The UND site was located at the approximate center of the surface sensor network.

A list of 131 microbursts which impacted the surface sensor network is presented. Particular emphasis is on the 107 events for which both radar data and surface data were available. Of these events, 14 were not observed by the surface network, while two events were not identified as microbursts by radar. Possible explanations of these missed microburst identifications are presented. The first case was an instance of the radar viewing a weak, asymmetric event from an unfavorable viewing angle. The second case describes an extremely shallow microburst outflow occurring at a height too low to be observed by the lowest elevation scan of the radar. In each of these cases, the featured microburst was very weak and, although a microburst-strength differential velocity was not observable by radar, in both instances the divergent wind pattern associated with the event was clearly evident in the radar velocity data field. All microbursts which exhibited a differential velocity of in excess of 13 m/s were identified by radar. No microbursts went unobserved as the result of insufficient signal return.

TABLE OF CONTENTS

LIST OF ILLUSTRATIONS

LIST OF ILLUSTRATIONS (continued)

LIST OF TABLES

ACRONYMS

FAA	Federal Aviation Administration
FL–2	FAA/Lincoln Laboratory TDWR Testbed Doppler Radar
FLOWS	FAA/Lincoln Laboratory Operational Weather Studies
LLWAS	Low-level Windshear Alert System
MIST	MIcroburst and Severe Thunderstorm (Project)
PAM	Portable Automated Mesonet
PROBE	Portable Remote OBservations of the Environment
TDWR	Terminal Doppler Weather Radar
UND	University of North Dakota
UT	Universal Time (same as Greenwich Mean Time)

I. INTRODUCTION

During 1986, Doppler radar and surface weather data were collected in Huntsville, AL as part of the FAA Terminal Doppler Weather Radar (TDWR) program [Evans and Johnson, 1984]. The primary objective of the project is to investigate the detectibility and predictability of low-level wind shear events in order that an automated alert system may be developed and implemented operationally. Of particular importance is the horizontal wind shear associated with microbursts, which are strong, small-scale downdrafts producing divergent outflow winds at or near the ground. These divergent winds have been shown to be a potential hazard to aviation [Fujita, 1980; National Research Council, 1983; Fujita, 1985]. The use of Doppler radar has been presented as a potentially effective method of detecting such wind shear events [Wilson, et al., 1984]. This report investigates the observability of microbursts using Doppler radar, through a comparative analysis of the 1986 Huntsville radar and surface sensor data.

Radar data were collected from two radars during the period of April through December 1986. The radars used were an S-band radar (FL-2) developed and operated by Lincoln Laboratory for the FAA [Evans and Turnbull, 1985] and a C-band radar operated for the FAA by the University of North Dakota (UND). The FL-2 radar was located just outside the northwest perimeter of the Huntsville Airport, while the UND radar was located approximately 15 km to the northwest of the airport (see Figure I-1).

Surface weather data were collected from three separate (but overlapping) networks of surface sensors which collectively covered an area of nearly 1000 square km centered approximately 15 km to the northwest of the airport. Data were collected during the period of April through December 1986 from two of the three networks: the FAA/Lincoln Laboratory Operational Weather Studies (FLOWS) surface mesonet consisting of 30 PROBE (Portable Remote OBservations of the Environment) weather stations [Wolfson, et al., 1986], and the network of 6 Low-Level Windshear Alert System (LLWAS) sensors surrounding the Huntsville Airport. The data collected by the PROBE mesonet included measurements of barometric pressure, relative humidity, temperature, precipitation rate, average and peak wind speed, and average wind direction; the LLWAS sensors recorded wind speed and direction only. Together these two networks covered an area of approximately 500 square km, with an average station spacing of approximately 3 to 5 km. During the period of June-July 1986, surface sensor data were also collected by the NCAR second generation Portable Automated Mesonet (PAM II) network [Pike, et. al., 1983] of 41 stations as part of the Microburst and Severe Thunderstorm

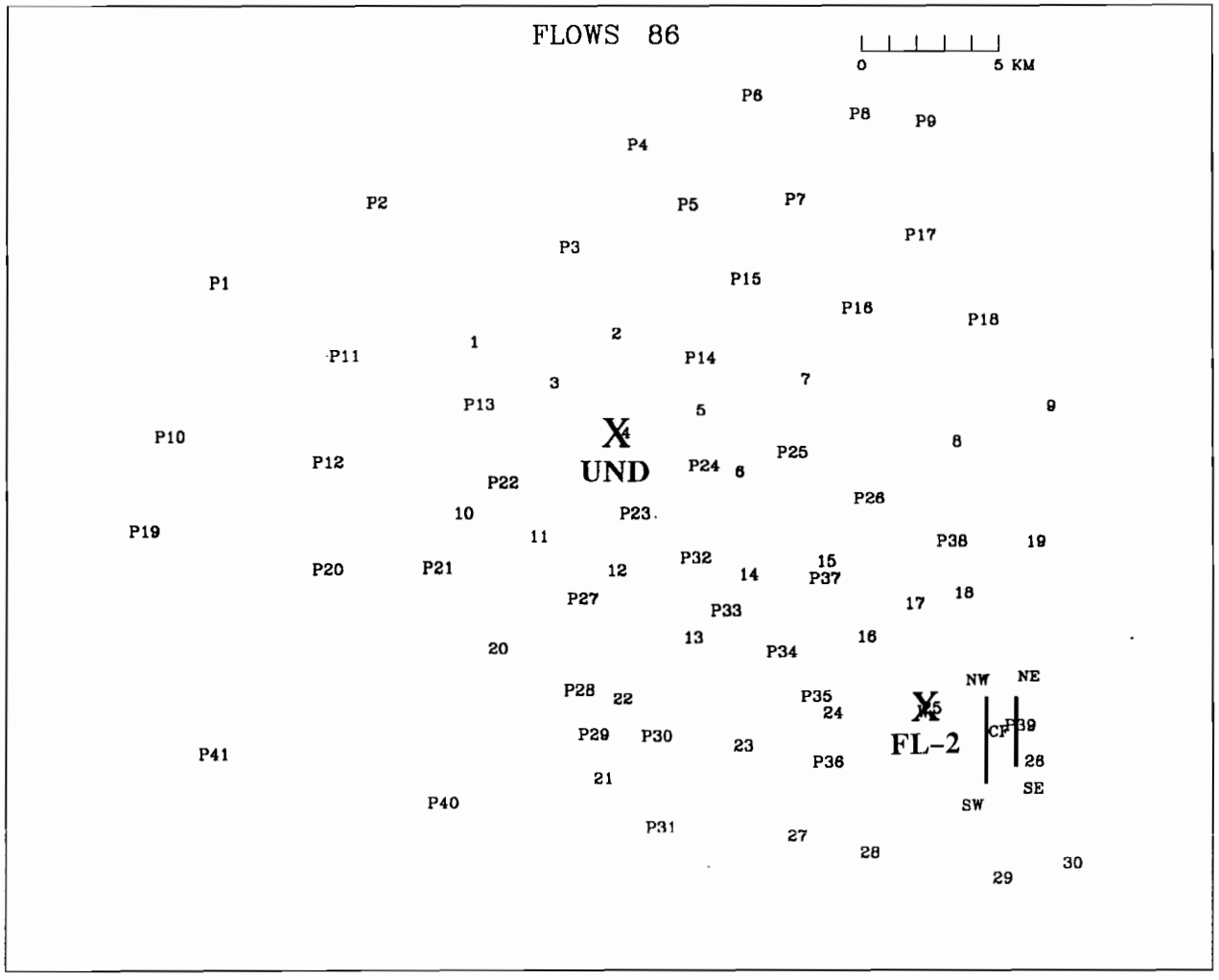

Figure I–1. The 1986 mesonet at Huntsville, AL. FL–2 and UND radars marked by X. FLOWS surface stations numbered 1 through 30; PAM stations numbered P1 through P41. LLWAS stations labeled with ordinal direction (NW, NE, etc.). Two solid lines represent location of Huntsville Airport runways.

(MIST) project [Dodge, et al., 1986]. These sensors collected measurements of the same meteorological parameters as the PROBE stations, and their inclusion during June and July extended the total areal coverage of surface data to approximately 1000 square km. It also increased the station density such that in the densest portion of the network (within 20 km to the north and west of the FL-2 radar) it was comparable to that of the enhanced Denver LLWAS system currently under development, with a typical distance of 1 to 4 km between stations. Outside of this area, the typical distance between stations was considerably less, ranging from 4 to 8 km. The locations of all 77 surface stations, as well as the runways of the Huntsville Airport, are also shown in Figure I-1. The three surface networks will henceforth be referred to collectively as the "mesonet".

This report focuses on the observability of microbursts which impacted the mesonet of surface sensors in the Huntsville area during the 1986 data collection period. In contrast to other studies which assess microburst algorithm detection performance, particularly as applied to the developmental TDWR system [Merritt, 1987], the approach here is to investigate the observability of microburst divergence signatures in Doppler radar velocity fields as associated with divergences observed at the surface by the mesonet. This distinction is illustrated in Figure I-2. The objective of this study is to examine the frequency with which a microburst may be undetectible by a radar-based system, not because of a failure of algorithms to correctly interpret a velocity field, but rather because the wind shear occurring near the surface is not observable in the velocity field. This report addresses the possibility that such events may be unobservable due to effects such as (1) low signal-to-noise ratio, (2) the radar beam scanning too high above surface divergence features, and/or (3) asymmetry in the surface wind field resulting in an underestimation of the low-level divergence [Eilts and Doviak, 1986].

Chapter II of this report describes the methodology used in identifying a microburst through analysis of both radar and mesonet data. Chapter III provides a summary of observed microbursts and results of radar/mesonet comparisons. Chapter IV focuses more closely on particular events which were not identified by radar. Chapter V provides a summary of conclusions, and Chapter VI presents a discussion of plans for continued data analysis.

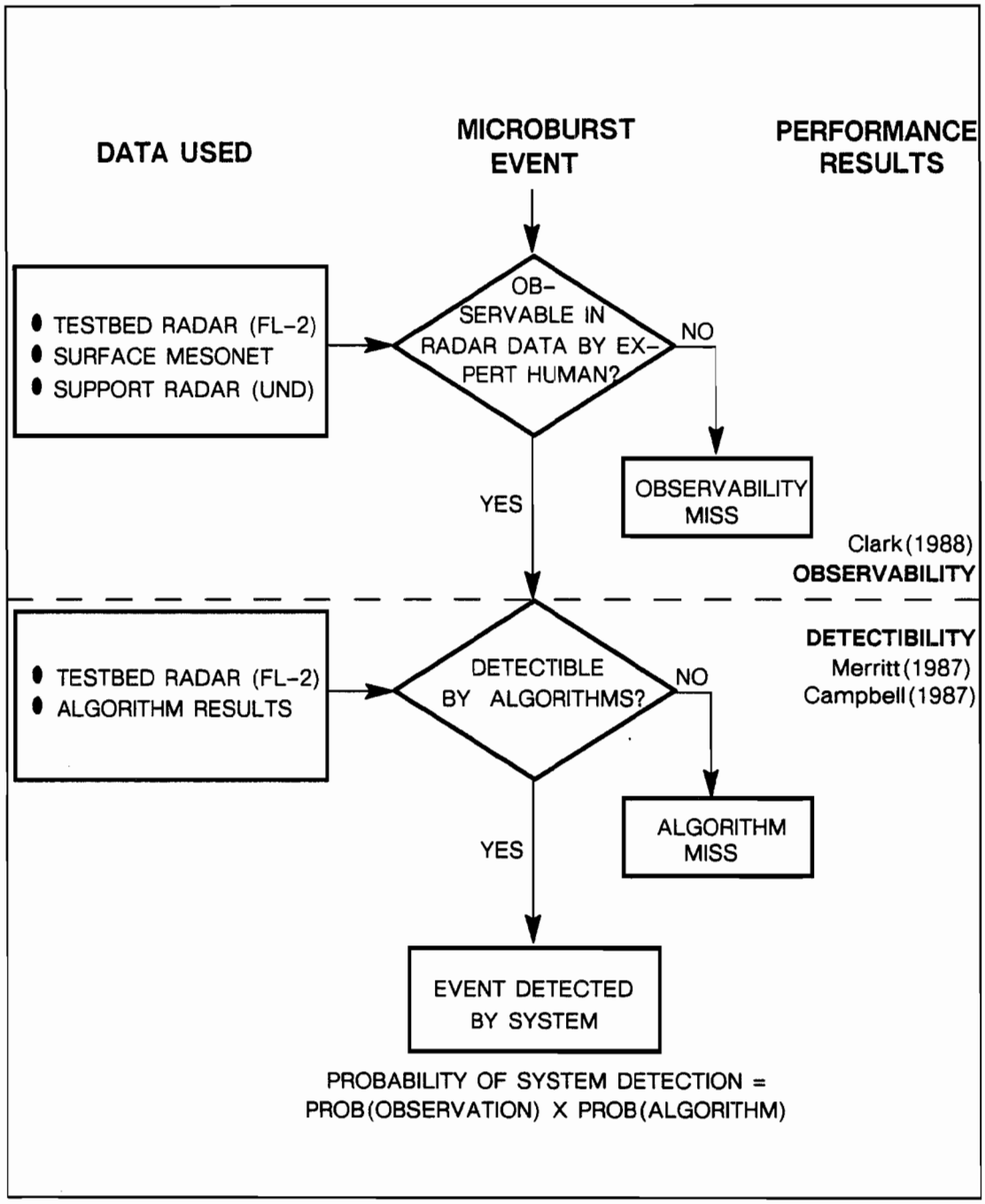

Figure I–2. Relationship between studies of microburst observability (upper portion) and microburst algorithm detectibility (lower portion.)

II. METHODOLOGY FOR MICROBURST IDENTIFICATION

This chapter describes the criteria and procedures used to identify microbursts using Doppler radar and surface sensor data.

A. Microburst Definition

A downburst is described [Fujita, 1985] as "a strong downdraft of damaging winds on or near the ground." The outflow winds from such an event are highly divergent and may be either straight or curved. Fujita subdivides downbursts according to their horizontal scale of damaging winds, where the term "macroburst" is used to describe a large downburst with outburst winds extending in excess of 4 km horizontally, while "microburst" is used to describe a small downburst whose damaging outflow winds extend no more than 4 km. This distinction is important in that the wind shear produced by a microburst is on a scale that is more likely to pose a hazardous threat to aviation. Analysis of radar and surface data involved detection of this divergent wind shear as the primary identifying feature of microbursts.

B. Microburst Identification Using Radar Data

Doppler radar allows viewing of the radial component of wind velocity as represented by the motion of hydrometeors and other atmospheric particles. The microburst signature is identified in the radial velocity field as a divergent outflow at or near the ground. This signature appears as a couplet of adjacent approaching (negative) and receding (positive) radial velocities, usually embedded within some larger scale mean flow. An idealized sketch of a divergent velocity couplet is shown in Figure II-1. Observation of this divergent pattern in both real time and playback modes was used as an indication of a microburst event. In order for an event to be classified as a microburst, it had to exhibit a minimum velocity differential of 10 m/s within a horizontal range of no more than 4 km along a radial extending across the outflow area. This criterion provides a threshold similar to those which are currently being used in operational microburst detection algorithms. However, the algorithms typically apply additional requirements, such as tests for spatial and temporal continuity [Merritt, 1987] and association between features at the surface and those aloft [Campbell, 1988]. Also, the data analysis performed by meteorologists to assess algorithm performance applies the same differential velocity threshold as that presented here; their methodology is somewhat less constraining, however, as measurements are allowable across a velocity couplet whose orientation is offset from the radial direction.

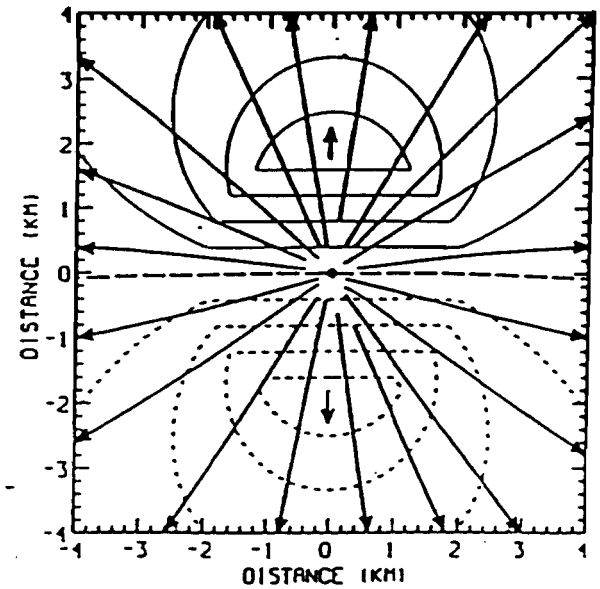

Figure II–1. Idealized sketch of radial velocity couplet, as viewed by radar from south (bottom of page). Heavy solid arrows indicate wind streamlines. Dashed lines and thin solid lines represent contours of positive and negative radial velocity, respectively.

The FL–2 radar was used as the primary source for radar data in identifying microbursts. However, UND radar data was used when FL–2 data was not available, or if an event identified by the surface mesonet went unobserved by FL–2. For each microburst, the time of maximum differential velocity exhibited in the radar data analysis was recorded. It should also be noted that the scanning sequence used in 1986 often included a number of range–height scans and high–elevation scans which resulted in a slow update rate of low–elevation scans (4–5 minutes), thus diminishing the temporal resolution of available data. As a result, the observability of a small percentage of events was deemed inconclusive, and were catagorized with those events for which no radar data was available. Scanning strategies currently in use provide a faster update rate (approximately once per minute), thus minimizing this limitation.

C. Microburst Identification Using Surface Data

Surface sensor mesonet data is received at Lincoln Laboratory and converted to a common format for further processing [Wolfson, et al., 1986]. For each day of data, values of the various meteorological parameters are plotted on a 24–hour time series graph for each station. These plots were analyzed for evidence of shear events, with the primary indicator being a sharp

peak in wind speed at one or more stations, accompanied by a change in wind direction. Other indicators include an abrupt change in temperature, pressure, and/or relative humidity, as well as the occurrence of precipitation. More detailed information on these indicators is discussed by Fujita [1985] and Rinehart, et al. [1986]. Once potential shear events were identified from the 24-hour plots, a series of one-minute wind barb plots (indicating wind speed and direction) were analyzed for the appearance of surface divergence. As with the radar data, a divergence of at least 10 m/s across a distance of no more than 4 km was necessary in order to classify an event as a microburst. This was determined by examining the divergent area for at least one pair of stations showing a minimum differential velocity of 10 m/s using the wind component along a line through the station pair (Figure II-2):

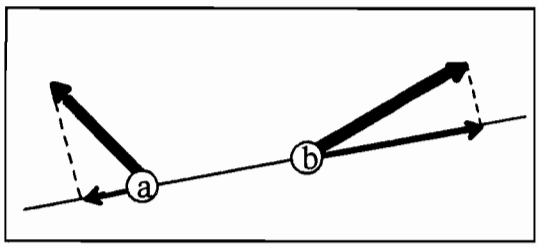

Figure II-2. Wind components measured along a line through stations a and b, used for differential velocity calculations.

In areas of the mesonet where the station spacing was greater than 4 km, formal calculations were performed to determine whether the area of divergent winds exhibited the necessary horizontal shear of at least 2.5×10^{-3} s^{-1} , equivalent to a 10 m/s differential velocity across 4 km. These criteria were required to be maintained for at least 2 minutes in order for an event to be classified as a microburst. For each microburst, the duration for which a surface wind divergence was apparent (not necessarily above threshold) was noted.

The reliability of the methodology described herein as a suitable approach for microburst identification was supported through comparison with a parallel study performed under the direction of T. Fujita at the University of Chicago using a subset of the 1986 Huntsville data. Their methodology was based on an objective single-station detection algorithm [Fujita, 1985]. Results from the two studies showed consistency in identifying microbursts, with most discrepancies easily explainable by the differing characteristics of the two identification approaches (peak wind threshold - vs. - surface divergence threshold).

III. SUMMARY OF RESULTS

A total of 131 microbursts were identified which impacted the surface mesonet area. A complete listing is presented in Table III-1. For each microburst, the table indicates the date, time period of surface divergence, identification by surface mesonet and/or radar, location with respect to indicated radar, approximate maximum velocity differential measured by radar, values of negative/positive velocity couplet, and the time at which the radar observed maximum differential velocity. The approximate location of each microburst is plotted in Figure III-1.

A statistical summary of microbursts detected is as follows:

Total Microbursts Identified	131
No Radar Data Available	24
Radar Data Available	107
Identified by Both Mesonet and Radar	91
Identified by Radar Only	14
Identified by Mesonet Only	2

Of primary significance to this study are the 107 events for which both radar data and surface mesonet data were available for comparison. As indicated, there were 16 events which were not identified by both the surface mesonet and the radar. 14 of these events were "misses" by the mesonet. These 14 events can be further subdivided as follows:

Microbursts Identified by Radar Only	14
Divergence Observed	6
Insufficient Spacing	3
Event Occurred at Mesonet Periphery	3
No Divergence Observed	8
Insufficient Spacing	8
Event Occurred at Mesonet Periphery	0

Table III-1
1986 Huntsville Mesonet Impacting Microbursts

Time refers to duration of divergent surface winds as observed by mesonet. Mesonet Identification: Y=Yes, N=No, D=Divergence (below microburst threshold) only. Radar Identification: FL-2/UND=identified by indicated radar, N=No, ND=No Data. Location is range/azimuth with respect to cited radar (or FL-2, when no radar is cited). Maximum ΔV, couplet values, and time of maximum ΔV are as observed by radar.

MB#	Date	Time (UT)	Identified by: MESO	RADAR	Approx. Location (km, deg)	Approx. Max ΔV (m/s)	Approx. Couplet (m/s)	Max ΔV Observ. Time(UT)
1	6 Apr	1839–1914	Y	FL-2	16,265	14	-15,-1	1838
2	24 May	1143–1220	D	FL-2	11,360	12	-2,+10	1159
3	27 May	1933–1957	Y	FL-2	4,285	15	-8,+7	1942
4	27 May	2008–2030	Y	FL-2	13,300	12	-2,+10	2008
5	1 June	2120–2213	Y	FL-2	4,305	15	-12,+3	2201
6	1 June	2201–2216	Y	N	12,310	--	--	2201
7	2 June	1729–1812	Y	ND	12,305	--	--	--
8	2 June	1733–1830	Y	ND	14,340	--	--	--
9	3 June	1847–1908	Y	FL-2	19,260	12	-2,+10	1854
10	3 June	1855–1909	Y	FL-2	15,280	12	-3,+9	1857
11	3 June	1910–1930	Y	FL-2	19,315	21	-4,+17	1911
12	3 June	1909–1933	Y	FL-2	20,310	16	-1,+15	1917
13	3 June	1937–1950	D	FL-2	23,340	12	-4,+8	1942
14	7 June	1704–1718	Y	FL-2	18,260	22	-18,+4	1705
15	7 June	--	N	FL-2	12,340	16	-5,+11	1721
16	7 June	1719–1727	Y	FL-2	7,360	19	-3,+16	1721
17	8 June	2103–2118	Y	ND	21,305	--	--	--
18	8 June	2136–2200	Y	ND	12,250	--	--	--
19	8 June	2218–2233	Y	FL-2	8,195	16	-12,+4	2225
20	8 June	2230–2241	Y	FL-2	5,330	11	-1,+10	2240
21	8 June	2248–2259	Y	FL-2	15,265	14	-4,+10	2253
22	8 June	2252–2322	Y	FL-2	7,295	12	-1,+11	2254
23	8 June	--	N	FL-2	18,270	14	-5,+9	2257
24	8 June	2246–2304	Y	FL-2	15,290	14	+1,+15	2257
25	8 June	2256–2304	Y	ND	12,260	--	--	--
26	8 June	2300–2333	Y	FL-2	10,280	16	-6,+10	2309
27	9 June	0815–0828	Y	ND	23,300	--	--	--
28	10 June	2028–2034	Y	FL-2	3,005	10	-1,+9	2029

Table III-1 (continued)

MB#	Date	Time (UT)	Identified by: MESO	RADAR	Approx. Location (km, deg)	Approx. Max ΔV (m/s)	Approx. Couplet (m/s)	Max ΔV Observ. Time (UT)
29	17 June	1943-2009	Y	ND	21,340	--	--	--
30	17 June	2000-2013	Y	ND	14,325	--	--	--
31	17 June	2006-2031	Y	ND	17,300	--	--	--
32	17 June	2008-2011	Y	ND	20,305	--	--	--
33	17 June	2012-2044	Y	ND	32,290	--	--	--
34	29 June	1157-1245	Y	FL-2	12,360	14	-4,+10	1237
35	29 June	1231-1257	Y	FL-2	17,280	13	-10,+3	1244
36	1 July	1800-1809	Y	FL-2	18,290	14	-13,+1	1804
37	1 July	1811-1840	Y	FL-2	9,295	18	-8,+10	1820
38	1 July	1816-1826	Y	FL-2	7,315	27	-17,+10	1820
39	1 July	1816-1830	Y	FL-2	10,305	14	-4,+10	1821
40	6 July	2032-2106	Y	FL-2	7,025	14	-9,+5	2051
41	11 July	0005-0015	Y	FL-2	23,340	12	-4,+8	0012
42	11 July	2004-2019	D	FL-2	28,310	14	-13,+1	2004
43	11 July	--	N	FL-2	26,290	15	-12,+3	2006
44	11 July	2004-2050	Y	FL-2	10,300	24	-18,+6	2031
45	11 July	2008-2038	Y	FL-2	24,285	16	-15,+1	2009
46	11 July	2008-2038	Y	FL-2	13,330	17	-11,+6	2032
47	11 July	2021-2034	Y	FL-2	24,330	15	-8,+7	2023
48	13 July	2010-2030	Y	FL-2	18,280	21	-23,-2	2015
49	13 July	2015-2021	Y	FL-2	16,305	17	-13,+4	2015
50	13 July	2019-2028	D	FL-2	26,280	18	-17,+1	2024
51	13 July	2016-2040	Y	FL-2	30,275	18	-22,-4	2028
52	13 July	2027-2038	Y	FL-2	6,265	13	-12,+1	2028
53	13 July	2028-2035	Y	FL-2	8,315	14	-11,+3	2028
54	13 July	2031-2041	Y	ND	22,295	--	--	--
55	13 July	2034-2048	Y	UND	12,085	18	-3,+15	2040
56	13 July	2036-2051	Y	UND	13,125	22	-10,+12	2040
57	13 July	2040-2048	Y	N*/(UND)	19,315	--	--	--
58	13 July	2040-2101	Y	FL-2	14,265	17	-12,+5	2051
59	13 July	2044-2109	Y	FL-2	7,265	28	-21,+7	2052
60	13 July	2057-2101	Y	FL-2	20,330	14	-7,+7	2058
61	13 July	2059-2112	Y	FL-2	17,315	21	-13,+8	2058
62	13 July	2103-2113	Y	FL-2	18,310	23	-22,+1	2113
63	13 July	2112-2117	Y	FL-2	16,315	26	-25,+1	2113

Table III-1 (continued)

MB#	Date	Time (UT)	Identified by: MESO	RADAR	Approx. Location (km, deg)	Approx. Max ΔV (m/s)	Approx. Couplet (m/s)	Max ΔV Observ. Time(UT)
64	13 July	2112–2121	D	FL-2	9,015	10	-12,-2	2118
65	14 July	0428–0440	Y	FL-2	20,335	17	-8,+9	0431
66	14 July	2340–2346	Y	ND	16,350	--	--	--
67	14 July	2348–2359	Y	ND	13,325	--	--	--
68	16 July	1831–1910	Y	ND	16,285	--	--	--
69	25 July	2136–2145	Y	UND	20,130	16	-19,-3	2136
70	25 July	2143–2159	Y	FL-2	6,140	18	-13,+5	2152
71	25 July	--	N	FL-2	5,030	12	-2,+10	2147
72	25 July	2147–2205	Y	FL-2	4,120	22	-13,+9	2152
73	28 July	1746–1805	Y	FL-2	14,280	13	-9,+4	1759
74	29 July	0127–0134	Y	FL-2	6,355	11	-8,+3	0134
75	29 July	0135–0149	Y	ND	7,320	--	--	--
76	29 July	0142–0147	Y	FL-2	3,070	18	-6,+12	0141
77	29 July	0201–0210	Y	ND	3,195	--	--	--
78	1 Aug	0247–0304	Y	FL-2	13,280	23	-17,+6	0252
79	1 Aug	0304–0320	Y	FL-2	16,295	14	-7,+7	0314
80	8 Aug	0002–0008	Y	FL-2	8,030	24	-7,+17	0007
81	9 Aug	1954–2031	Y	UND	20,130	16	-11,+5	2011
82	9 Aug	2009–2020	Y	UND	19,115	22	-14,+8	2011
83	10 Aug	2305–2330	Y	UND	17,132	10	-10,0	2320
84	10 Aug	--	N	UND	10,090	20	-6,+14	2311
85	10 Aug	2317–2326	Y	UND	15,110	14	-11,+3	2320
86	10 Aug	2317–2327	Y	UND	15,120	18	-8,+10	2320
87	10 Aug	--	N	UND	12,125	12	-7,+5	2328
88	10 Aug	2328–2355	Y	UND	14,105	14	-5,+9	2344
89	10 Aug	2343–0002	Y	UND	13,100	26	-13,+13	2351
90	10 Aug	2354–0000	Y	UND	12,145	16	-8,+8	0000
91	10 Aug	2358–0030	Y	UND	13,120	40	-27,+13	0007
92	11 Aug	0030–0057	Y	UND	17,160	23	-17,+6	0034
93	11 Aug	0039–0117	Y	UND	4,195	34	-23,+11	0043
94	11 Aug	0101–0112	Y	UND	13,155	11	-4,+7	0104
95	11 Aug	0104–0111	Y	UND	14,135	14	-5,+9	0104
96	11 Aug	0109–0119	Y	UND	13,155	18	-9,+9	0115
97	11 Aug	0116–0123	Y	UND	17,180	12	-9,+3	0120
98	11 Aug	0116–0123	Y	UND	15,135	13	-3,+10	0120

Table III-1 (continued)

MB#	Date	Time (UT)	Identified by: MESO	RADAR	Approx. Location (km, deg)	Approx. Max ΔV (m/s)	Approx. Couplet (m/s)	Max ΔV Observ. Time(UT)
99	11 Aug	0132-0152	Y	UND	20,125	14	-1,+13	0139
100	16 Aug	1751-1830	Y	UND	7,320	14	-4,+10	1818
101	16 Aug	1836-1933	Y	UND	18,155	24	-8,+16	1852
102	24 Aug	1837-1904	Y	FL-2	12,285	16	-7,+9	1853
103	24 Aug	1919-1949	Y	FL-2	22,280	24	-13,+11	1920
104	24 Aug	2123-2150	Y	FL-2	26,320	16	-9,+7	2105
105	25 Aug	2059-2131	Y	FL-2	17,330	10	-4,+6	2100
106	26 Aug	2029-2051	Y	UND	12,210	29	-17,+12	2026
107	26 Aug	2030-2045	Y	UND	12,230	15	-12,+3	2031
108	26 Aug	2056-2126	Y	UND	20,140	26	-8,+18	2109
109	28 Aug	0000-0011	Y	ND	18,330	--	--	--
110	28 Aug	0213-0224	D	UND	15,150	15	-3,+12	0213
111	12 Sep	0409-0414	Y	ND	11,290	--	--	--
112	21 Sep	1849-1859	Y	FL-2	11,290	13	-8,+5	1848
113	21 Sep	1854-1907	Y	FL-2	11,250	18	-7,+11	1853
114	21 Sep	1911-1923	Y	FL-2	13,255	20	-6,+14	1909
115	22 Sep	2239-2300	Y	FL-2	2,030	17	-11,+6	2239
116	22 Sep	2256-2259	Y	FL-2	1,125	26	-12,+14	2256
117	22 Sep	--	N	FL-2	8,300	11	-3,+8	2303
118	22 Sep	--	N	FL-2	7,310	12	-4,+8	2303
119	22 Sep	2301-2311	Y	FL-2	2,315	10	-1,+9	2303
120	22 Sep	2302-2319	Y	FL-2	2,210	12	-1,+11	2311
121	22 Sep	2306-2324	Y	FL-2	2,100	34	-19,+15	2306
122	26 Sep	1835-1843	Y	FL-2	4,110	15	-5,+10	1836
123	26 Sep	1836-1900	Y	FL-2	18,305	11	-13,-2	1836
124	2 Oct	0102-0128	Y	FL-2	15,305	12	-14,-2	0111
125	2 Oct	0121-0132	D	FL-2	8,020	15	-6,+9	0128
126	9 Oct	0015-0053	Y	ND	14,270	--	--	--
127	9 Nov	0930-0953	Y	ND	16,305	--	--	--
128	20 Nov	0338-0401	Y	ND	15,320	--	--	--
129	20 Nov	1215-1300	Y	FL-2	18,305	11	-5,+6	1226
130	23 Nov	2246-2303	Y	ND	17,315	--	--	--
131	23 Nov	2310-2359	Y	ND	9,330	--	--	--

* MB #57 unobservable by FL-2, but observable by UND

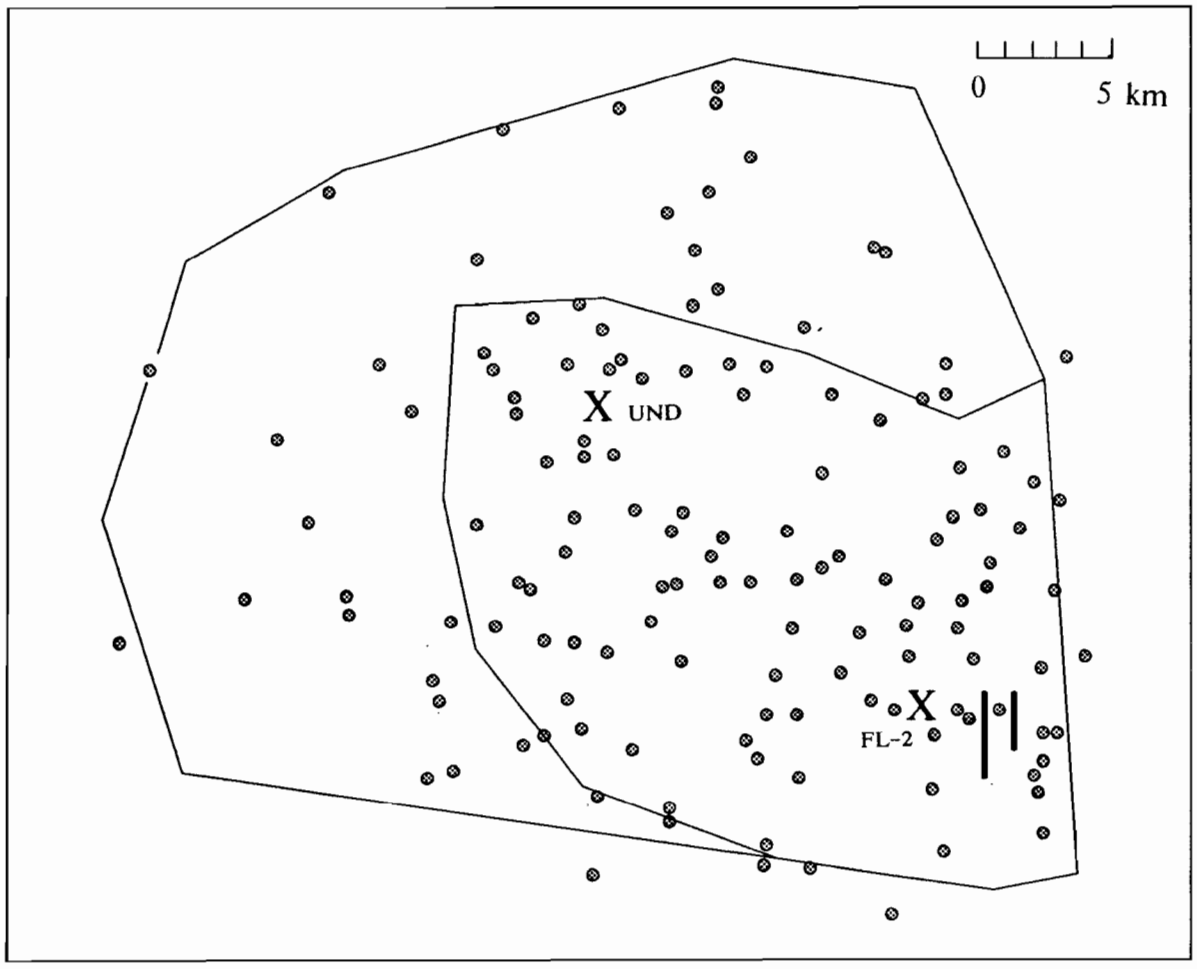

Figure III-1 Approximate locations of the 1986 mesonet impacting microbursts. Outer and inner thin solid lines indicate approximate perimeter of mesonet, including and excluding PAM stations, respectively. Heavy solid lines represent location of Huntsville Airport runways. FL-2 and UND radars marked by X.

As noted, six of the 14 events exhibited some degree of wind divergence, but the magnitude did not reach the prescribed threshold. Three times this underestimation was attributed to the event occurring in an area of the mesonet, as identified by radar, where the density of surface stations was not sufficient to resolve the full divergence of the event. The other three of these events did not reach threshold because the event occurred along the outer periphery of the mesonet where, although the event was centered inside the boundary of the mesonet, the full divergence associated with the event extended beyond the boundary of the mesonet, and was unobservable by surface sensors. Also as indicated, eight events showed no appreciable wind divergence due to an insufficient density of surface sensors. It should be noted that while these events did not show a wind divergence between stations, three of the events did cause a notably high wind gust at a single station, only one of which, incidentally, would be identified as a microburst by Fujita's single-station algorithm [Fujita, 1985].

Of the 107 events for which radar data was available, two events (1.9%) were not classified as microbursts as observed by radar. They include:

MB#	Date	Time(UT)	Location wrt FL-2 (km,deg)	ΔV Detected by: Mesonet	Radar
6	1 June	2201-2216	12,310	12 m/s	7 m/s
57	13 July	2040-2048	19,315	13 m/s	8 m/s

The first event (MB #6) was an instance in which the surface mesonet observed a differential velocity of just over the threshold of 10 m/s within 4 km, while the corresponding radar data showed a value just under this threshold. The second event (MB #57) was a special case in which the event was not identified by FL-2, but was identified by UND. These two cases are examined in detail in Chapter IV.

IV. CASE STUDIES OF MICROBURSTS NOT IDENTIFIED BY RADAR

A. Case 1: 01 June 1986

This case describes a microburst event which occurred approximately 12 km to the northwest of FL-2 from 2201-2216 UT, and was not identified as a microburst by the FL-2 radar. The microburst was very weak and short-lived, as it maintained a differential velocity above threshold for only two minutes with a maximum value of just 12 m/s. A microburst-strength velocity difference was not observed by the FL-2 radar, although the divergence associated with the event was apparent in the radial velocity field. The missed identification appears to be the result of asymmetry in the microburst outflow, with FL-2 viewing the event from an unfavorable angle.

Figure IV-1 is a plot of wind speeds and directions as measured by the surface sensors. The surface divergence signature was first seen at 2201 UT (Figure IV-1a) near station P23, with the maximum differential velocity observed between stations P24 and P32. The maximum differential velocity for the entire event occurred at 2203 UT (Figure IV-1b), also measured between stations P24 and P32. After 2203 UT, the microburst gradually weakened as it moved to the east, until the divergence signature was no longer apparent at 2217 UT. The maximum divergent shear and differential velocity for the event is plotted as a function of time in Figure IV-2. The microburst exhibited a maximum differential velocity of 12 m/s, and remained above threshold for just a couple of minutes.

The maximum shear as observed by the FL-2 radar occurred at 2201 UT (Figure IV-3). Two microburst-producing cells are seen to the northwest of FL-2 at that time (Figure IV-3a) at ranges of 4 km and 12 km. Of interest to this case is the furthermost cell, which shows a maximum reflectivity factor of 50-55 dBz, with typical values of 40-50 dBz in the microburst outflow region. A divergence signature associated with the event can be seen in the velocity field (Figure IV-3b), and is most evident near 10 km range where there is an area of negative velocities of approximately -9 m/s. The other half of the divergent couplet is not readily apparent, however, and the maximum differential velocity attained within 4 km was 7 m/s, as verified by analysis of the raw radial velocity data. Unfortunately, no UND radar data from this date is available for comparison.

The missed identification by FL-2 in this case appears to be the result of an unfavorable viewing angle of a short-lived event of marginal strength. As described above, the maximum differential velocity as measured by the mesonet was detected at 2203 UT between stations P24 and P32, a station pair

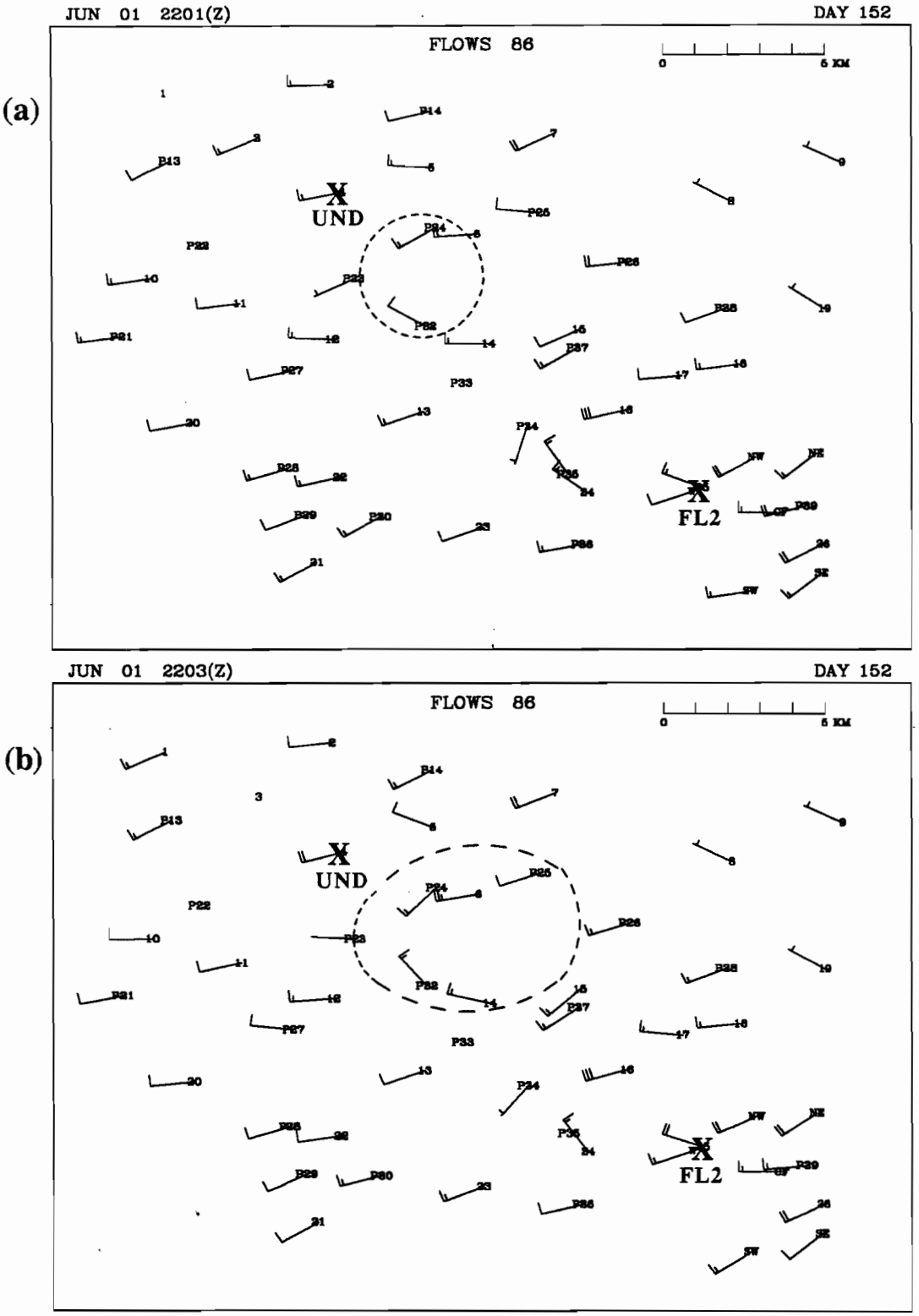

Figure IV-1. Mesonet plots showing the surface wind field for 1 June 1986 at (a) 2201 UT and (b) 2203 UT. Full barb equals 5 m/s; half-barb equals 2.5 m/s. Dashed line represents approximate microburst outflow boundary. Location of FL-2 and UND radars marked by X.

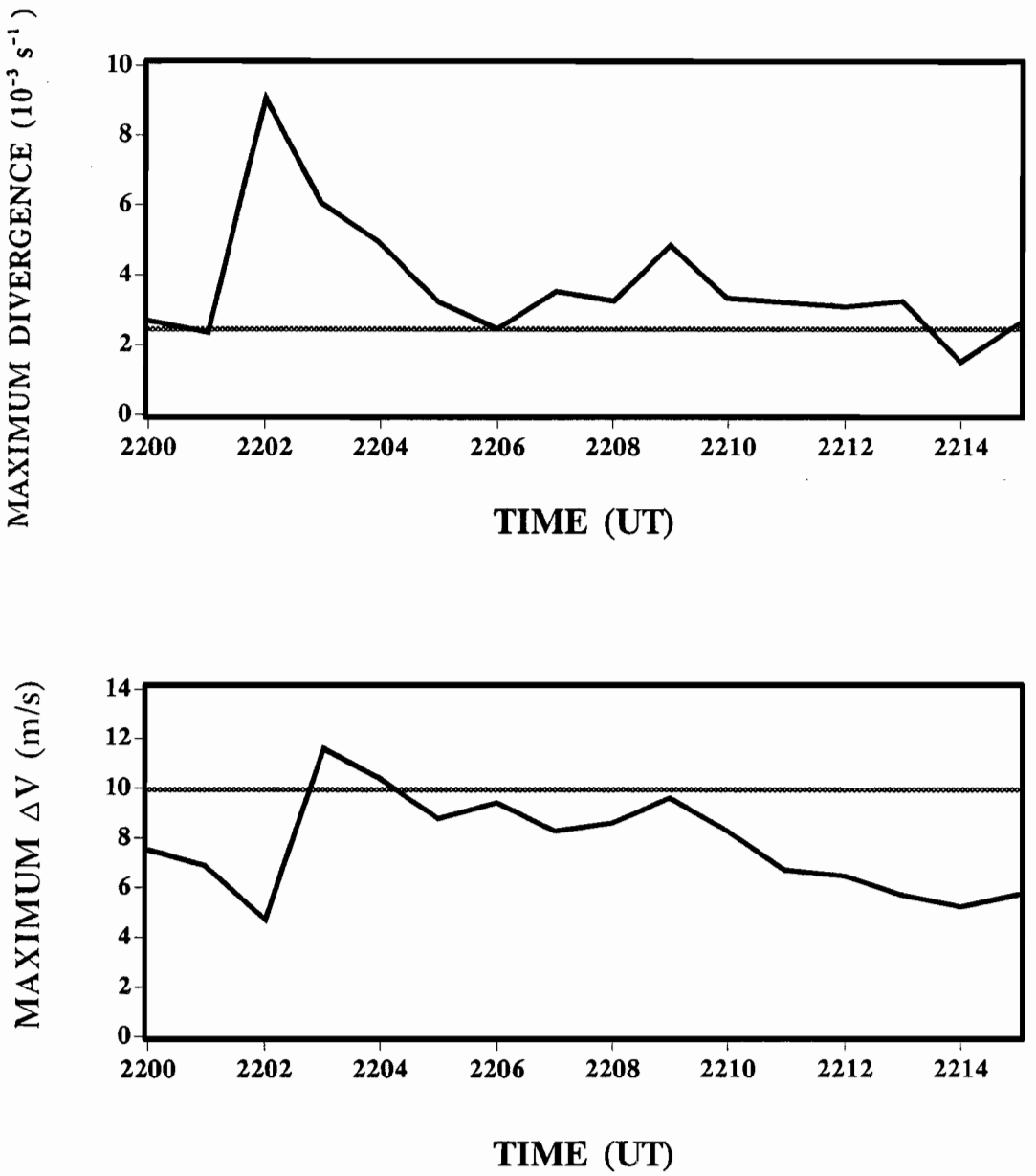

Figure IV-2. Maximum divergence and differential velocity values computed over mesonet using actual measured winds for times specified on 1 June 1986. Horizontal lines indicate microburst threshold values.

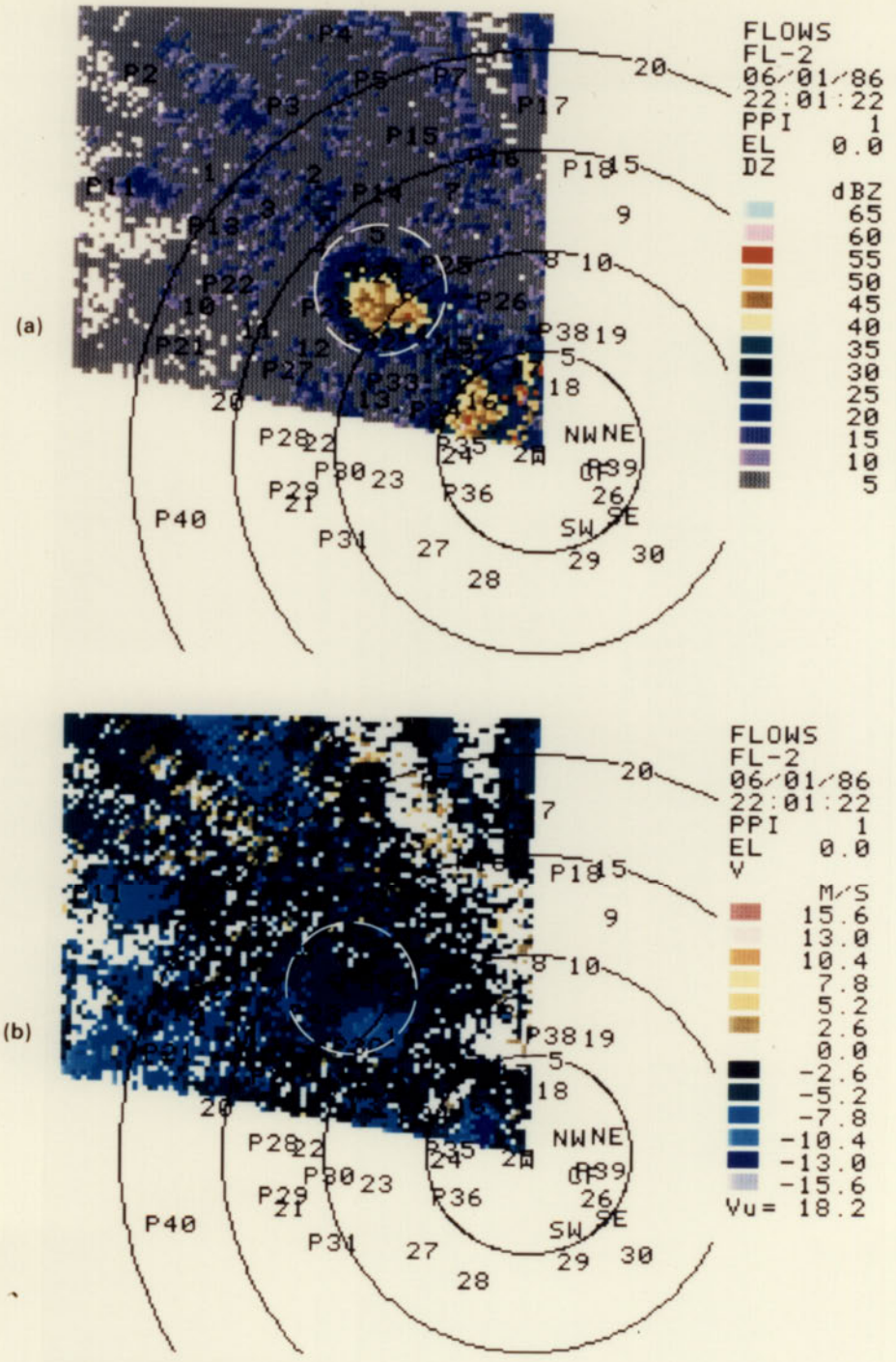

Figure IV-3. FL-2 radar (a) reflectivity and (b) Doppler velocity fields for 1 June 1986 at 2201 UT. Elevation angle is 0.0 degrees for both plots. Range rings are every 5 km from FL-2. FLOWS surface stations labeled 1 through 30; PAM stations labeled P1 through P41; LLWAS stations labeled with ordinal directions. White dashed circle represents approximate microburst outflow region.

with a north–south orientation. From 12 km to the southeast, the FL–2 radar was viewing the axis of this station pair at an angle of approximately 45 degrees, while measuring a lesser differential velocity (7 m/s) along a radial oriented northwest–southeast. This suggests the possibility of a microburst with an asymmetric outflow shear being viewed by FL–2 from an unfavorable angle. To investigate asymmetry as observed by the mesonet, differential velocity was measured along four different axes running through the center of the microburst, with one of the axes oriented along a radial from FL–2 (Figure IV–4). The mesonet wind field was used to estimate the maximum differential velocity observable within a 4 km distance across these axes. Where necessary, values of wind direction and speed along the axes were interpolated from the actual winds of surrounding stations to yield the best estimate of maximum differential velocity along each axis. At 2201 UT (Figure IV–4a), the maximum differential velocity is estimated at 6 m/s along the north–south axis. This agrees quite well with the maximum station pair differential velocity difference of 5 m/s measured between P24 and P32, as plotted previously in Figure IV–2. At 2203 UT, the velocity difference measured between these two stations reached a maximum of 12 m/s; correspondingly, the difference measured along the north–south shear axis at this time (Figure IV–4b) is 13 m/s, and it represents the largest value along any of the four axes. The asymmetry in the shear is clearly apparent at this time, with the minor axis of differential velocity oriented northwest–southeast, estimated at a value of 7 m/s. Thus FL–2 was observing the microburst from just about the least favorable viewing aspect possible. To test the integrity of the FL–2 measurements, the mesonet wind field was plotted using only the wind component of each station along a radial from FL–2 (Figure IV–5). The figure confirms the maximum velocity difference observable by FL–2 as a 7–8 m/s couplet oriented northwest–southeast, in accordance with the FL–2 shear estimate. Therefore the effect of viewing an asymmetric shear event from an unfavorable aspect, in an instance of such minimal microburst strength, appears responsible for the missed identification by the FL–2 radar.

Previous studies [Eilts and Doviak, 1987; Wilson, et al., 1984] suggest that asymmetric microburst outflows such as that described here are not uncommon, with typical asymmetry ratios (major shear axis versus minor shear axis) on the order of 2:1. Given the frequency of this characteristic, one issue has been the relative infrequency of missed radar detections due to this effect, particularly in light of the significant proportion of weak or "marginal" microbursts. For example, of the 107 events identified in this study for which a radar–mesonet comparison could be made, nearly half (46%) exhibited a maximum differential velocity of less than 15 m/s (see Table IV–1), yet only

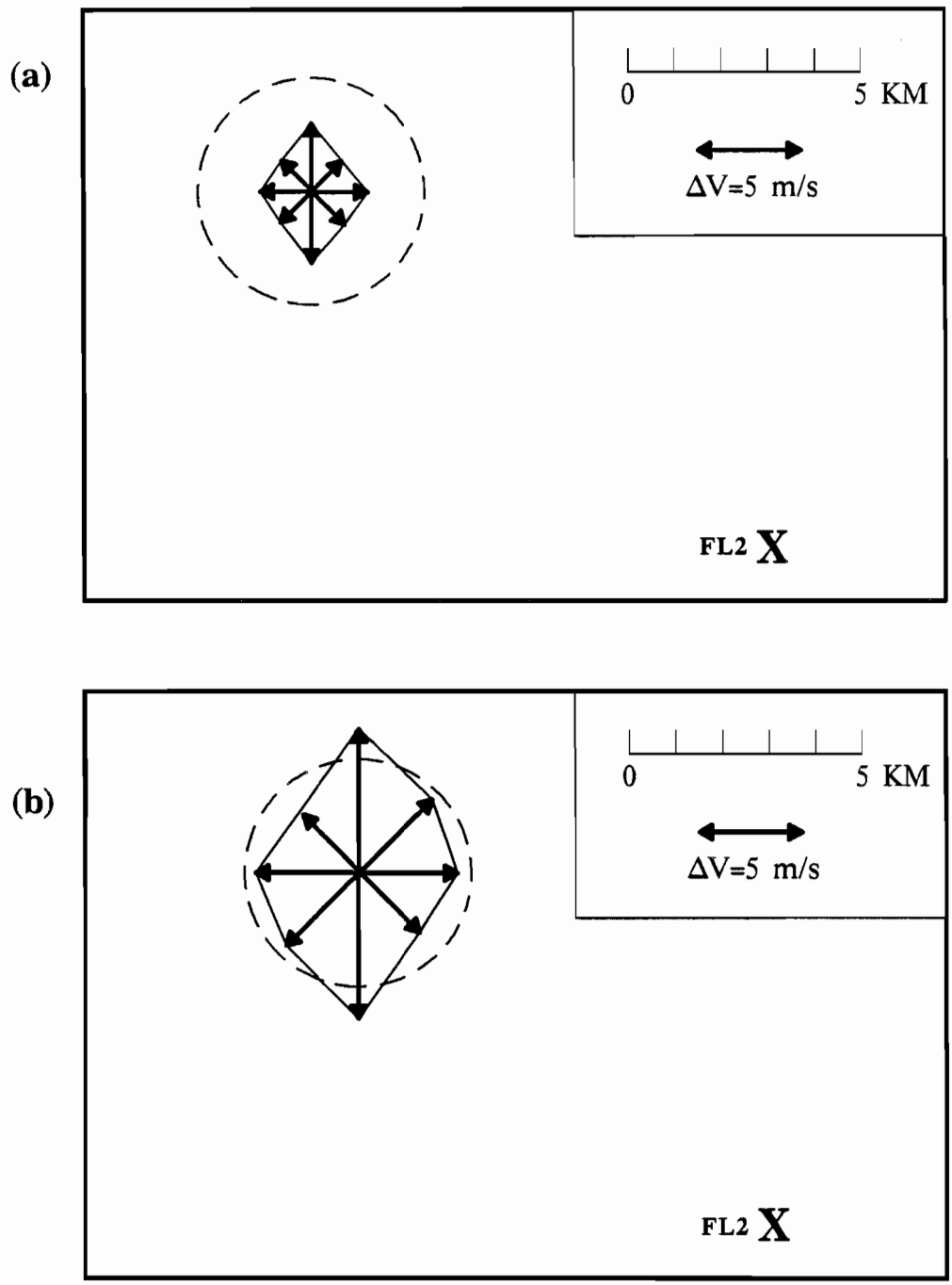

Figure IV-4. Maximum differential velocity within 4 km distance along axes through center of microburst at (a) 2201 UT and (b) 2203 UT on 1 June 1986. Length of each axis proportional to differential velocity in m/s as indicated by scale. Dashed line denotes threshold of 10 m/s. Location of FL-2 radar marked by X.

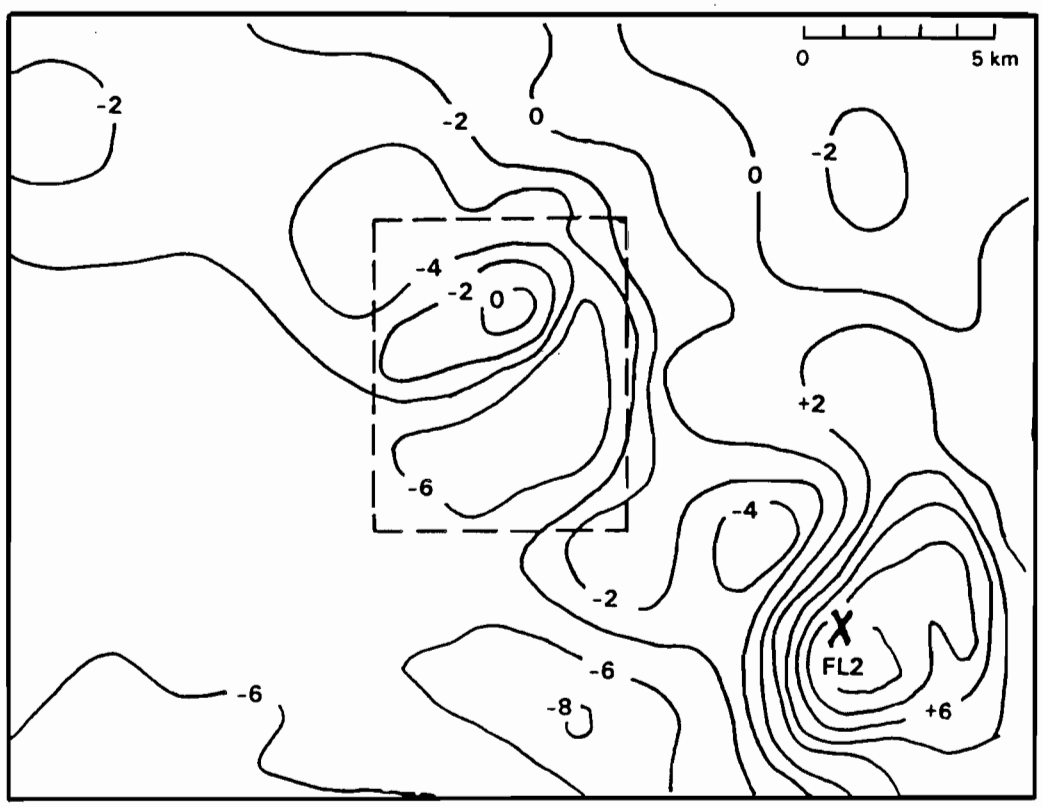

Figure IV-5. Radial component with respect to FL2 radar of mesonet-measured wind field for 2203 UT on 1 June 1986, in m/s. Location of FL2 radar marked by X.

Table IV-1. Frequency Distribution of Microbursts by Maximum Differential Velocity

ΔV (m/s)	Frequency	Percentage
10–14	49	46%
15–19	32	30%
20–24	15	14%
25–29	8	7%
30+	3	3%

one of these microbursts was not identified as a microburst because of asymmetry. In a similar study by DiStefano [1987], 12 of 42 microbursts (29%) had a maximum velocity difference of less than 15 m/s, of which only one was not identified by radar with asymmetry cited as a contributing factor. One possible explanation of this observation would be that a positive correlation exists between microburst strength and asymmetry, with asymmetry less likely to be a characteristic of weak microbursts. However, this relationship has not been supported by evidence to date [Wilson, et al., 1984; personal communication, Anderson, Hallowell]. The suggestion presented here is that this observation may be the result, at least in part, of limitations in the radar–mesonet comparisons, particularly with respect to the large difference in spatial resolution offered by the two sensing methods. With a typical surface station spacing of 1–4 km at best, the mesonet is attempting to estimate the magnitude of a feature using a resolution of approximately the same spatial scale as the feature itself. Under these circumstances it is unlikely that, for a given event, the maximum differential velocity detected by the mesonet will have been measured between a pair of stations whose axis runs through the center of the microburst outflow. Thus the "truth", as determined by the mesonet, is very likely to yield an underestimate of the actual maximum wind shear magnitude. The resultant effect is that the weak microbursts identified by the mesonet are actually not as "marginal" as the estimated differential velocities would lead one to believe. In contrast, the radar has the advantage of observing the same event using a spatial resolution on the order of 0.12–0.25 km in range, less than 0.5 km azimuthally within 30 km range (assuming a 1 degree half-power beamwidth), and less than 0.25 km azimuthally within a range of 15 km. This provides a spatial resolution as much as 30 times finer than that of the mesonet. The result is that a radar azimuth is significantly more likely to pass through (or nearer) the microburst outflow center than is the axis of a mesonet station pair, with an additional advantage in capturing the maximum shear through high resolution measurements in range. This advantage in spatial resolution by the radar is at least partially compensating for its limitation in estimating the magnitude of an asymmetric event. Given a mesonet of infinite station density (or at least a density which provides the spatial resolution of the radar), the speculation is that a considerably higher number of "truly" marginal events would likely be identified, events for which the radar would not have a resolution advantage, thus decreasing the radar observation percentage of *weak* microbursts.

B. Case 2: 13 July 1986

This case was unique to this study in that it portrays an instance in which a microburst was observed by the surface sensor network, was not identified by the FL-2 radar, but was identified by the UND radar. The microburst was weak and extremely shallow, with a microburst-strength outflow limited to a height of approximately 100 meters. Closer proximity to the event provided the UND radar with a lower viewing height than FL-2, and this appears to have made the difference in observability.

The event occurred from 2040-2048 UT near stations #1, #2, and P3, approximately 19 km northwest of the FL-2 radar and 4 km northwest of the UND radar. Surface wind speeds and directions are depicted in Figure IV-6. At 2042 UT (Figure IV-6a), the microburst is evidenced by a backing wind at station #1, and an increase in wind speed at station P3 from 7.5 m/s to 12.5 m/s. By 2045 UT (Figure IV-6b), the microburst was seen as a divergence in wind between stations P3 and #2. By 2049 UT, all evidence of the event as seen by the surface network is gone. The event was brief (9 minutes) and covered a small areal extent.

Time series plots of both maximum divergent shear and maximum differential velocity for the event are shown in Figure IV-7.As indicated, the maximum differential velocity went slightly above the threshold of 10 m/s from 2041-2042 UT, dropped below threshold at 2043 UT, and increased to a maximum of 13 m/s at 2045 UT. Maximum divergent shear also peaked to a value of 3.7×10^{-3} s^{-1} at 2045 UT, which is above the prescribed threshold of 2.5×10^{-3} s^{-1} .

The earliest available FL-2 radar data is a 0.3 degree elevation scan at 2045 UT (Figure IV-8). A large reflectivity cell is seen near stations #1 and #2 (Figure IV-8a), with maximum values of 45-50 dBz, and values ranging from 30 to 50 dBz in the microburst outflow region. The corresponding radial velocity data is shown in Figure IV-8b. A divergent couplet is apparent in the area of the microburst event; however, the couplet orientation is rotated counterclockwise from the radial direction (with respect to FL-2), indicating anticyclonic rotation within the cell. A 10 m/s differential velocity within 4 km distance was not attained along a radial. Figure IV-9 shows the raw radar data prior to conversion to a Cartesian grid, and allows closer inspection of the radial velocity field. A +3 to +4 positive velocity maximum is highlighted near 22 km range. An area of relative maximum velocity of -4 to -5 m/s is shown radially from the positive area (azimuth=313 degrees) near 16 km, which corresponds to an 8 m/s shear across a radial distance of 6 km. A second

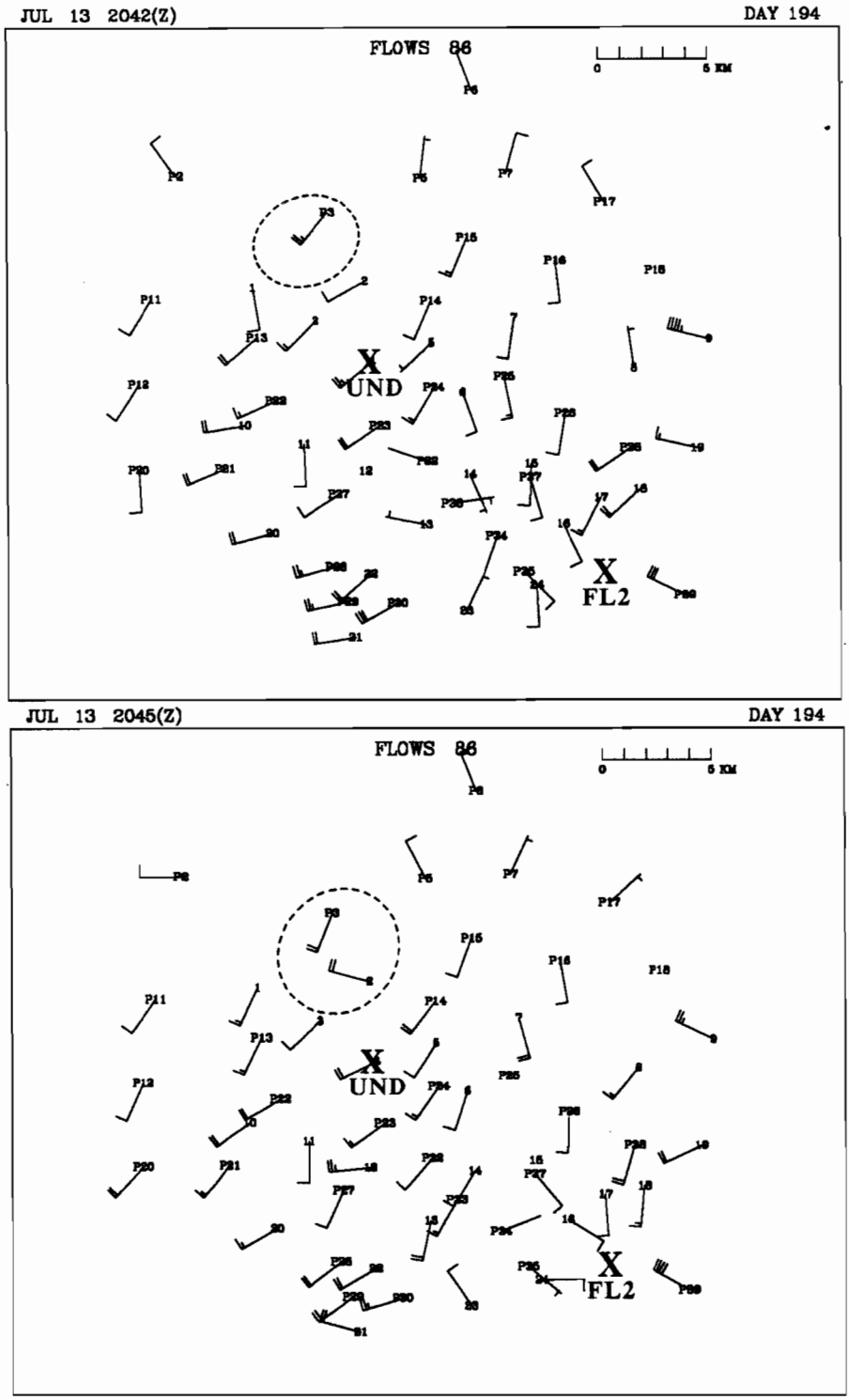

Figure IV-6. Mesonet plots showing the surface wind field for 13 July 1986 at (a) 2042 UT and (b) 2045 UT. Full barb equals 5 m/s; half-barb equals 2.5 m/s. Dashed line represents approximate microburst outflow boundary. Location of FL-2 and UND radars marked by X.

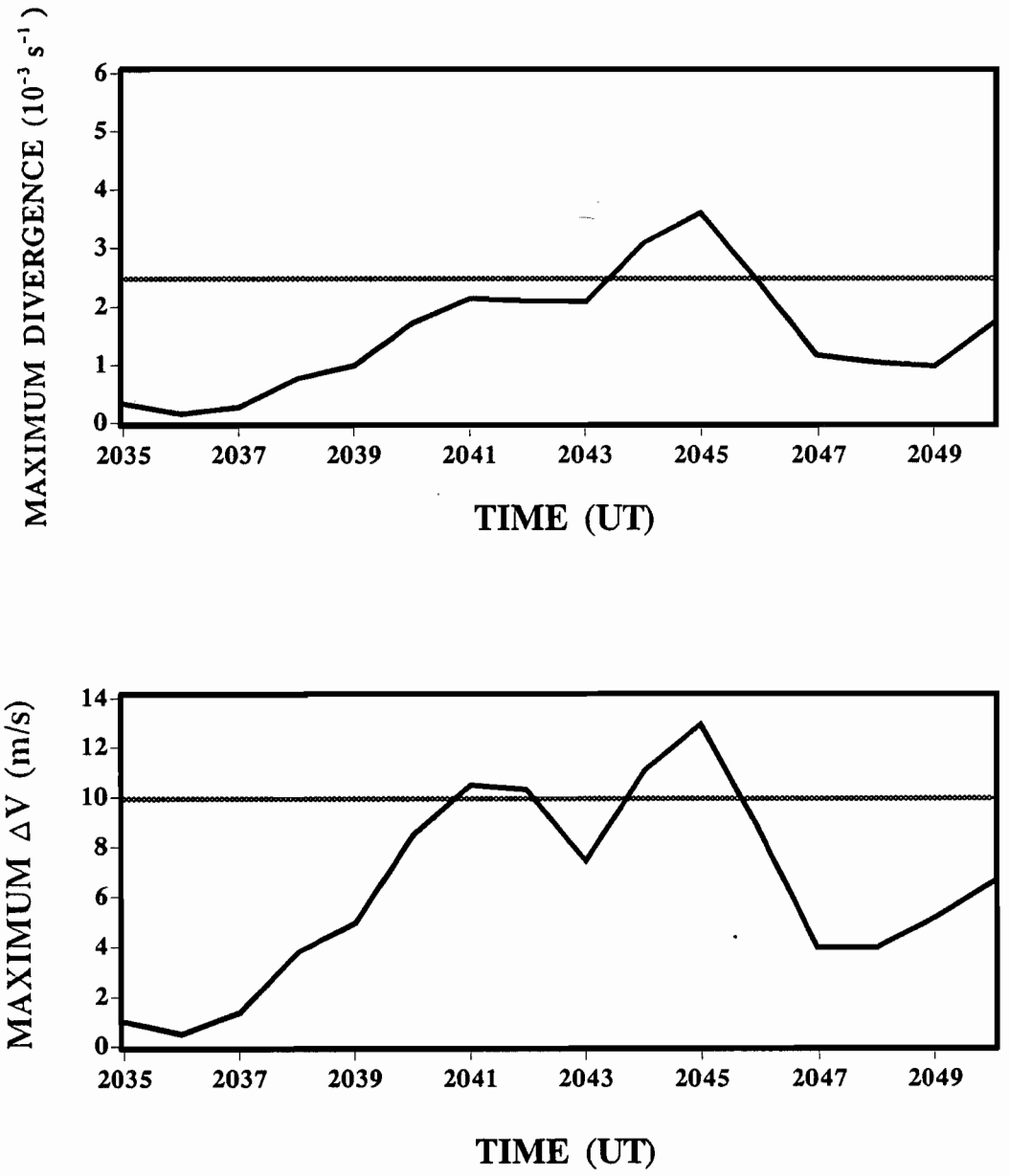

Figure IV–7. Maximum divergence and differential velocity values computed over mesonet using actual measured winds for times specified on 13 July 1986. Horizontal lines indicate microburst threshold values.

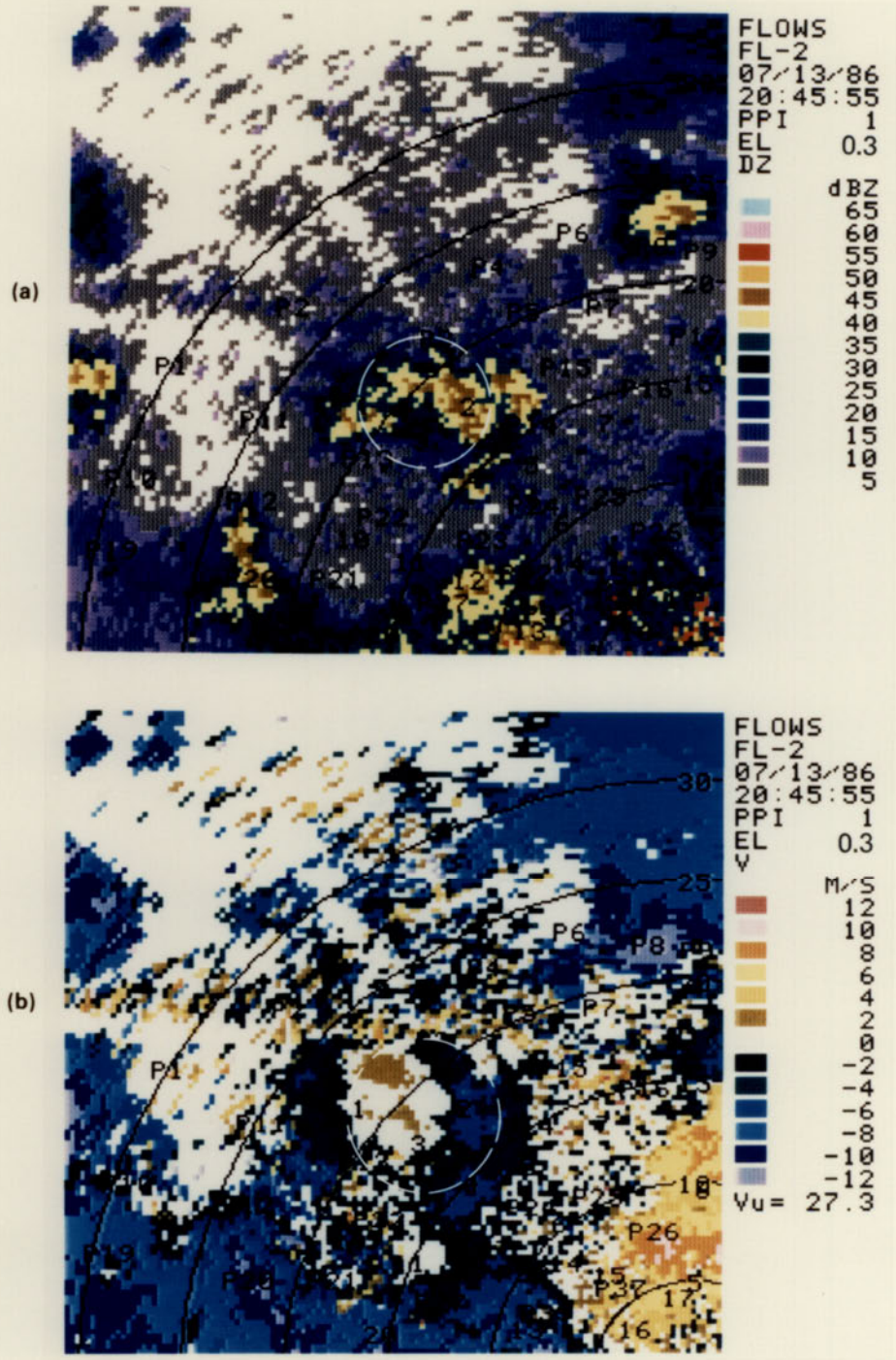

Figure IV-8. FL-2 radar (a) reflectivity and (b) Doppler velocity fields for 13 July 1986 at 2045 UT. Elevation angle is 0.3 degrees for both plots. Range rings are every 5 km from FL-2. Locations of FLOWS, PAM, and LLWAS surface stations are overlaid. White dashed circle represents approximate microburst outflow region.

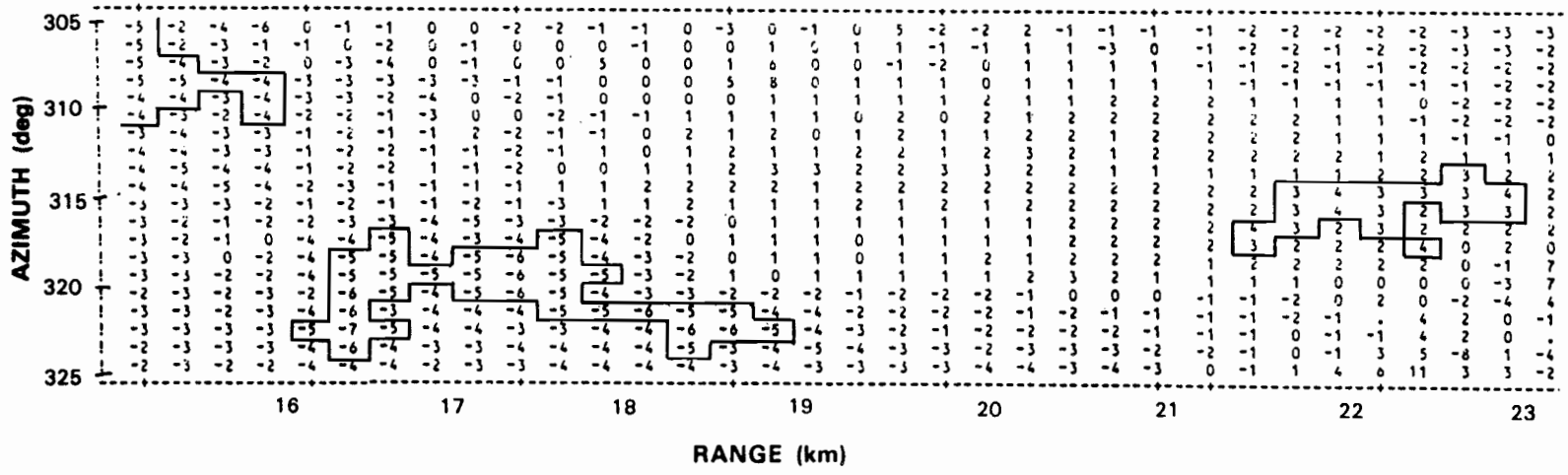

Figure IV–9. Doppler velocities in m/s as seen by FL–2 on 13 July 1986 at 2045 UT. Elevation angle is 0.3 degrees.

negative velocity relative maximum of -5 to -7 m/s is seen near 18 km range, but is not oriented radially from the positive maximum. This skewed couplet possibly would have been sufficient to declare a microburst as "truthed" in real-time by human analysis [personal communication, Isaminger]. However, looking radially outward from this second negative maximum yields a maximum differential velocity of only 8 m/s within 4 km, which does not qualify the event as a microburst as determined by the methodology employed in this study as described in Chapter II. Inspection of higher elevation angles also fail to indicate a sufficient shear, while exhibiting increased rotation with height.

Radar data from UND is available at both 2040 UT and 2045 UT. At 2040 UT, a clear microburst signature is apparent in the 0.4 degree elevation scan (Figure IV-10b), with a -8/+6 m/s couplet centered 6 km to the northwest of the UND radar site indicating a differential velocity of 14 m/s. Unfortunately, no FL-2 data is available for comparison at that time. At 2045 UT, the maximum reflectivity within the microburst-producing cell (Figure IV-11a) is in the 50-60 dBz range, which is some 5-10 dBz higher than as seen by FL-2, perhaps due to the difference in viewing height. The microburst signature can still be seen as a tight -7/+4 m/s couplet situated just west of station #2 (Figure IV-11b). This is verified by inspection of the corresponding raw radar data (Figure IV-12a). Analysis of higher elevation scans indicate rapid weakening of shear with height. At 1.5 degrees elevation, the shear drops just below microburst threshold. This is seen as a 9 m/s differential velocity as measured from the raw radial data (Figure IV-12b), with a velocity couplet of -4/+5 m/s found at approximately 340 degrees azimuth at a range of 5 km. Also note that the couplet at this elevation is displaced somewhat from the radial direction indicating rotation; at 2.5 degrees the signature is almost purely rotational.

The analysis indicates a maximum differential velocity of 13 m/s observed by the surface network at 2045 UT, 14 m/s observed by UND at 2040 UT decreasing to 11 m/s at 2045 UT, and 8 m/s observed by FL-2 at 2045 UT with no data available at 2040 UT. The deficiency in FL-2 data is due to a lightning strike near the radar site which disabled a local disk drive, resulting in a 14-minute gap of radar data during the critical period of 2031-2044 UT. Without this untimely outage, it is quite possible that the event would have been observable by FL-2 at 2040 UT, as supported by the higher shear value seen by UND at that time. Maximum differential velocity as measured by radar is typically attained sooner than the surface maximum, since it is sensing aloft a descending feature. If no UND data had been available for this event, as was the case for many of the events in this study, this case would not have

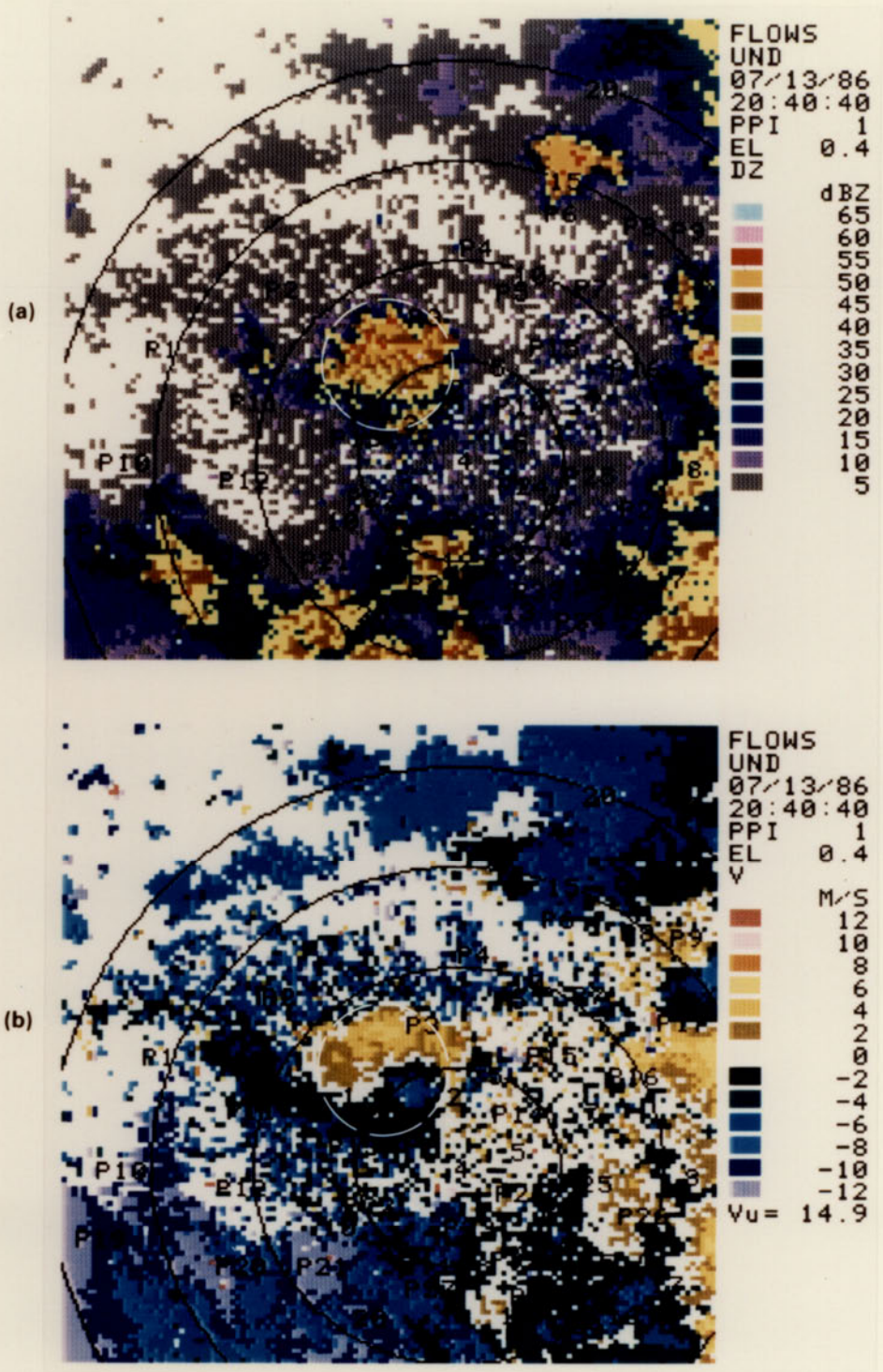

Figure IV-10. UND radar (a) reflectivity and (b) Doppler velocity fields for 13 July 1986 at 2040 UT. Elevation angle is 0.4 degrees for both plots. Range rings are every 5 km from UND. Locations of FLOWS, PAM, and LLWAS surface stations are overlaid. White dashed circle represents approximate microburst outflow region.

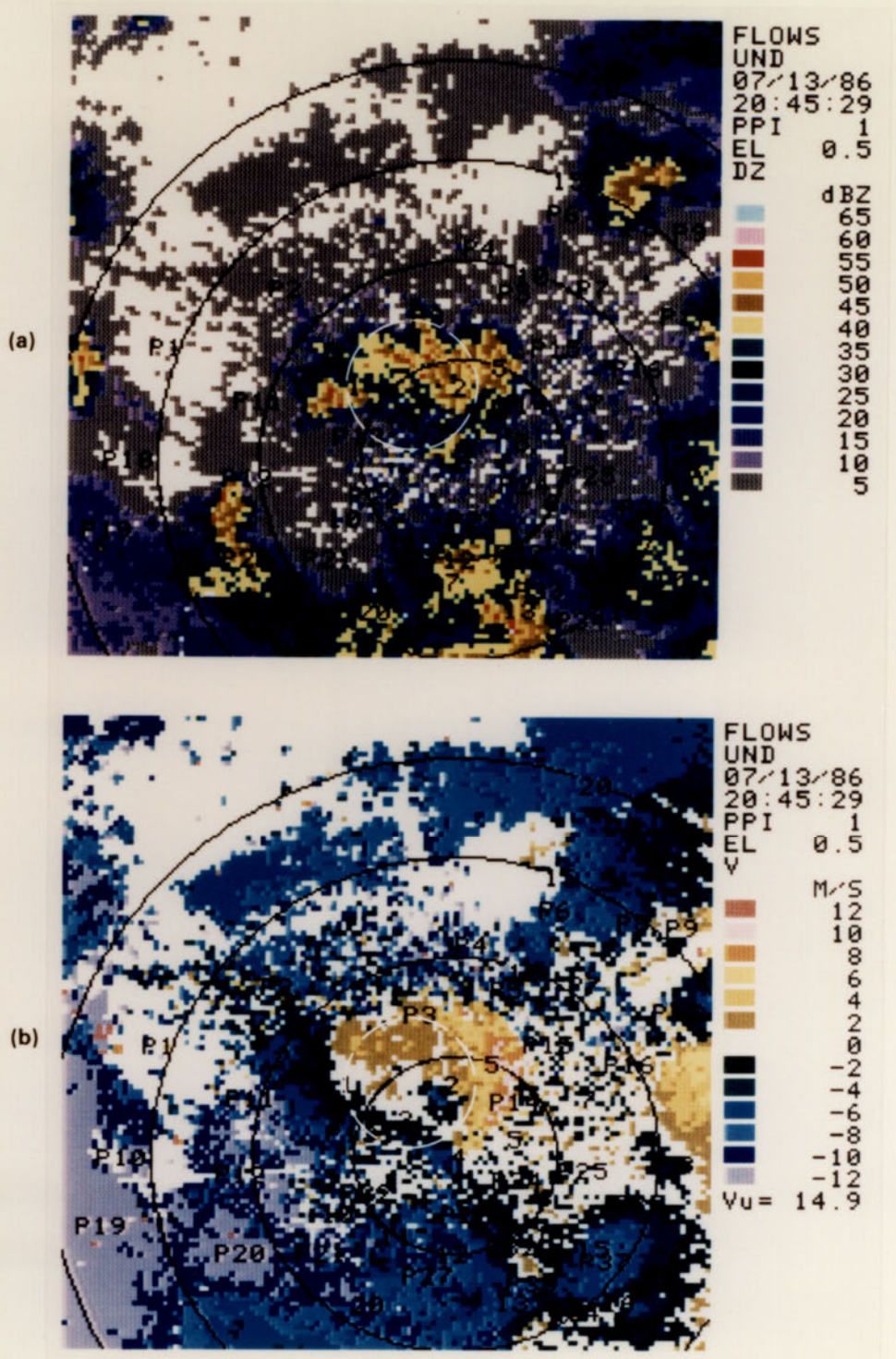

Figure IV-11. UND radar (a) reflectivity and (b) Doppler velocity fields for 13 July 1986 at 2045 UT. Elevation angle is 0.5 degrees for both plots. Range rings are every 5 km from UND. Locations of FLOWS, PAM, and LLWAS surface stations are overlaid. White dashed circle represents approximate microburst outflow region.

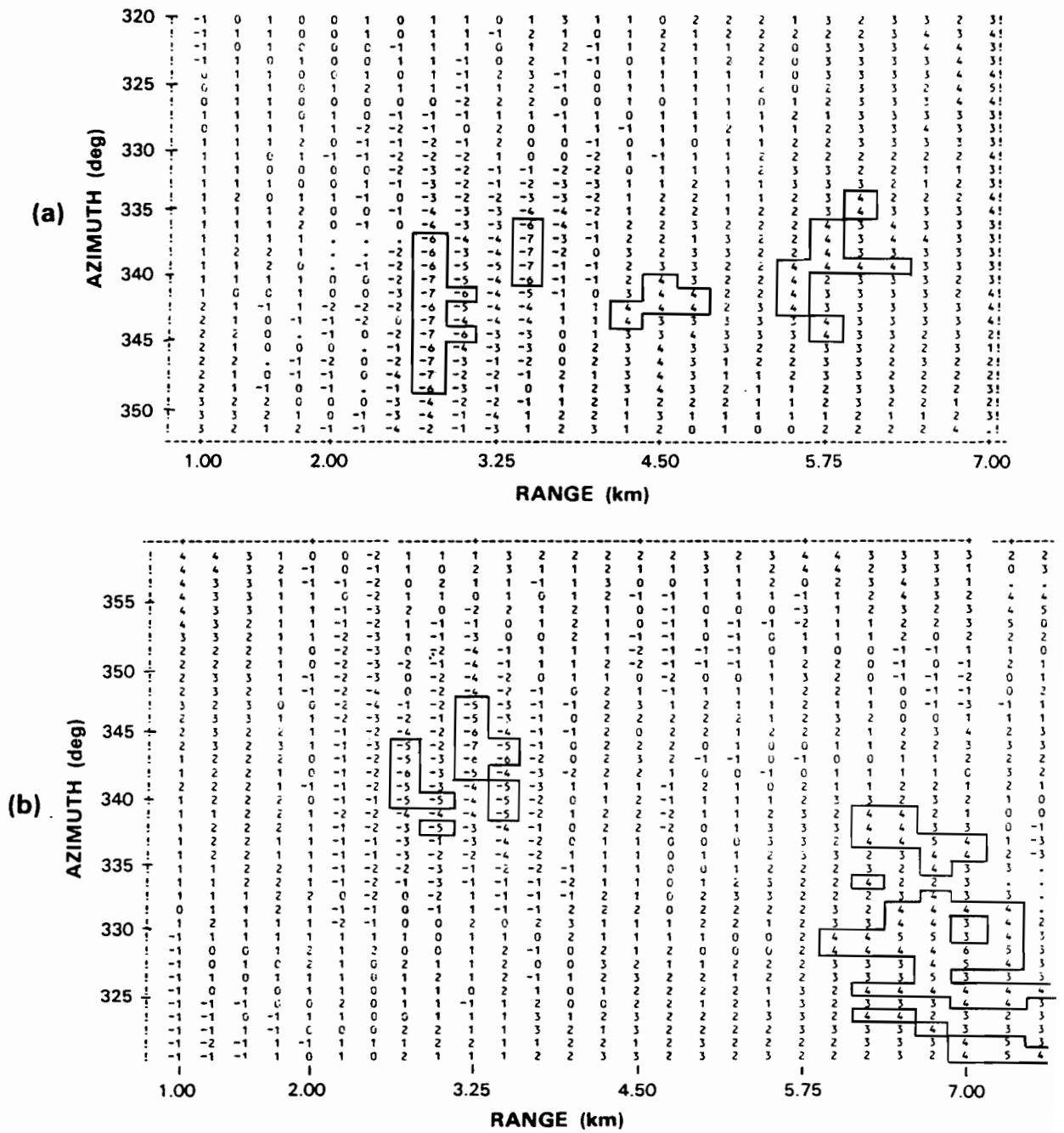

Figure IV–12. Doppler velocities in m/s as seen by UND on 13 July 1986 at 2045 UT. Elevation angles are (a) 0.5 and (b) 1.5 degrees.

been classified as a missed identification by FL–2 due to insufficient data availability.

Viewing aspects of the microburst were compared for possible explanations of the detection discrepancy between FL–2 and UND. Figure IV–13 illustrates the height of the low–elevation beams for the scans available from the two radars at 2045 UT. The microburst signature is seen strongest by UND at 0.5 degrees elevation (36 meters above ground level at 4 km range), weakens to just below the minimum shear threshold at 1.5 degrees (106 m), and becomes a rotation signature at 2.5 degrees (175 m) rather than a divergence signature. Thus the microburst–strength outflow was confined to an extremely shallow depth of approximately 100 meters, as compared to a more typical outflow depth of several hundred kilometers [Wilson, et al., 1984]. The lowest elevation scan available from FL–2 was at 0.3 degrees; at a range of 19 km, FL–2 was observing the event only as low as 121 meters above ground level, as indicated in the figure. With UND measuring a maximum differential velocity of 9 m/s at a height of 106 m and FL–2 measuring 8 m/s at 121 m, it is likely that the missed detection was due, at least in part, to the shallowness of the event.

Asymmetry was also considered as a possible source of difference in observations by the two radars at 2045 UT. However, the location of the microburst at that time was such that both radars had approximately the same azimuthal viewing angle (Figure IV–14). Maximum shear at the surface was measured as 13 m/s between stations #2 and P3; as the figure indicates, these stations are situated such that a favorable viewing angle (nearly along a radial) is allowed for both radars, with FL–2 having perhaps a slightly better aspect. This would discount the potential effect of viewing an asymmetric event, and favor the likelihood that the microburst was not identified by FL–2 due to its shallow depth.

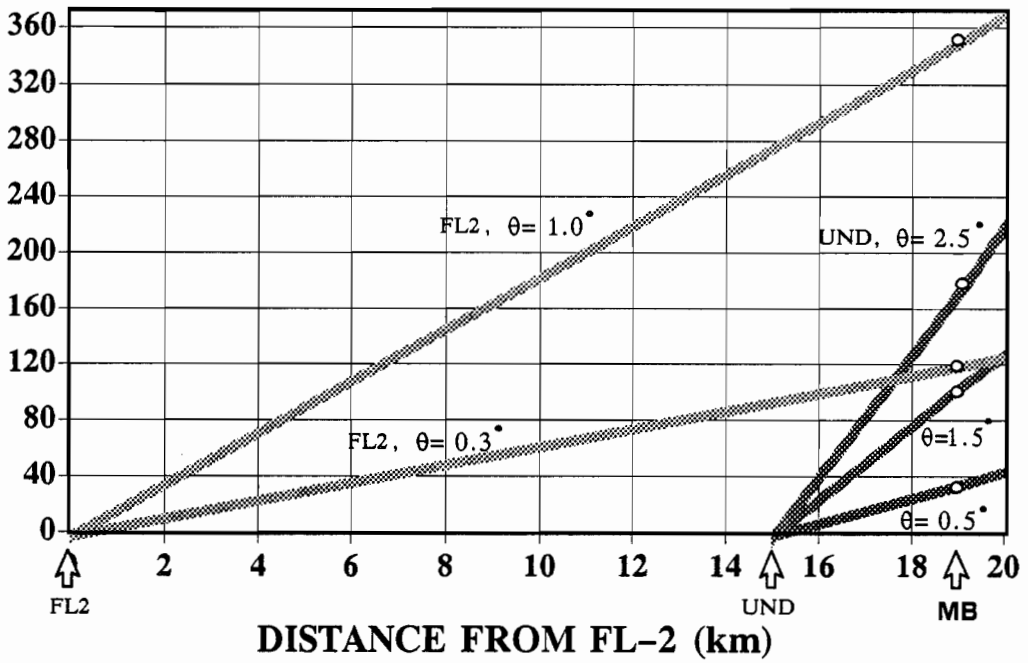

Figure IV-13. Height of radar beam above ground level for low-elevation scans from FL-2 and UND radars.

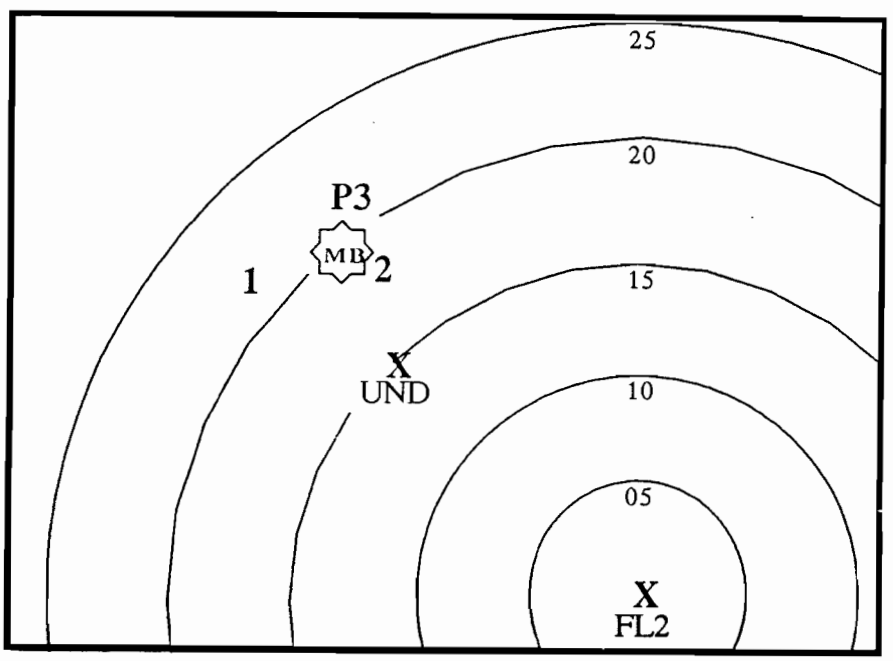

Figure IV-14. Location of microburst at 2045 UT on 13 July 1986 with respect to FL-2 and UND radars. Locations of surface stations #1, #2, and P3 are indicated. Range rings are every 5 km from FL-2.

V. CONCLUSIONS

A total of 131 microbursts impacted the 1986 Huntsville mesonet during the data collection period of April through December. There were 107 events for which both radar data and surface mesonet data were available for comparison. Of these, 91 (85%) were identified by both the radar and surface mesonet, 14 (13%) were identified by radar only, and 2 (2%) were identified by the surface mesonet only.

Of the 14 microbursts which were not identified by the surface mesonet, 11 were missed due to inadequate density of the surface sensors. The other three microbursts occurred along the periphery of the mesonet where the surface outflow away from the radar extended beyond the perimeter of the mesonet, thus not allowing the sensors to measure the full strength of the shear. Although failing to reach microburst threshold, six of the 14 missed events exhibited some degree of surface divergence.

Two of the 107 microbursts were not identified by radar, corresponding to an observation percentage of 98%. Both of these missed events were weak; no microburst exhibiting a differential velocity of greater than 13 m/s went unobserved by radar. The first missed event was the result of an unfavorable viewing angle of a short-lived asymmetric microburst of marginal strength. Surface sensors measured a maximum differential velocity of 12 m/s while the FL-2 radar, viewing nearly along the minor shear axis of the microburst, measured a maximum of 7 m/s across a distance of 4 km. The accuracy of the FL-2 shear estimation was supported by extraction of the radial component from the mesonet-measured wind field. The second event classified as a missed radar detection was a special case in which a microburst was identified by the UND radar but not by the FL-2 radar. The missed identification appears to be due to the extreme shallowness of the microburst-strength outflow, which extended to a height of approximately 100 meters. UND was able to identify the microburst due to its close proximity to the event which afforded a sufficiently low viewing height. Observations by both radars at a comparable height just above the event showed similar differential velocities of 8 to 9 m/s. FL-2 observation was also disadvantaged by lack of data earlier within the time span of the microburst. The sparse data availability provided only a single observation over the lifetime of the event. However, the availability of UND data nearly simultaneous with that of FL-2 was sufficient to confirm the occurrence of microburst-strength shear, and justified the classification of a missed identification by FL-2; the observability by FL-2 would otherwise have been deemed inconclusive due to insufficient data availability. Scan strategies currently in use for the testbed TDWR system provide more frequent low-elevation updates (approximately once per minute) which greatly reduces the likelihood of missed detection due to poor temporal resolution.

Insufficient signal-to-noise ratio did not pose a problem in the observation of 1986 Huntsville-area microbursts as no events were missed due to low reflectivity signal, a result consistent with the moisture-rich climate of the southeast United States. Both

microbursts not identified by radar were produced from convective cells exhibiting a maximum reflectivity factor in excess of 50 dBz. Typical reflectivity factor values in the microburst outflow region for these two cases ranged from 30 to 50 dBz.

VI. FUTURE WORK

Current plans include further comparison of radar and surface data, with focus on the time history relationship of microburst outflow winds as measured aloft by radar and at the surface by wind sensors. Since timeliness is critical to operational detection and warning of hazardous wind shear, a better understanding of this relationship will be important for assessing system performance and effectiveness. Of particular interest will be radar/surface comparisons of initial and final times of occurrence of microburst–strength shear, time and strength of maximum shear, and point estimates of wind speed and shear magnitudes. This information should also provide evidence to investigate the speculation presented in Section IV–A that the mesonet may be providing an underestimate of maximum wind shear strength as result of a spatial resolution inferior to that of radar. In addition, the planned deployment of TDWR requires development of methods to integrate the TDWR and LLWAS systems. The study proposed here will provide useful data to investigate:

(1) how alarms/data from the two systems may be combined.
(2) possible use of LLWAS data to refine headwind/tailwind estimates for TDWR–detected microbursts.
(3) the use of LLWAS data as an aid to TDWR in initial microburst detection.

REFERENCES

Campbell, S.D., 1988: Microburst Precursor Recognition Using an Expert System Approach. Preprints, Fourth International Conference on Interactive Information Processing Systems for Meteorology, Oceanography and Hydrology, Anaheim, CA, pp. 300–307.

DiStefano, J.T., 1987: Study of Microburst Detection Performance During 1985 in Memphis, TN. MIT, Lincoln Laboratory Project Report ATC–142, FAA Report DOT/FAA/PM–87–18, 25 pp.

Dodge, J., J. Arnold, G. Wilson, J.E. Evans, and T. Fujita, 1986: The Cooperative Huntsville Meteorological Experiment (COHMEX). Bulletin of the American Meteorological Society, **67**, 417–419.

Eilts, D.E., and R.J. Doviak, 1987: Oklahoma Downbursts and Their Asymmetry. Journal of Climate and Applied Meteorology, **26**, 69–78.

Evans, J.E., and D. Johnson, 1984: The FAA Transportable Doppler Weather Radar. Preprints, 22nd Conference on Radar Meteorology. Zurich, Switzerland, American Meteorological Society, pp. 246–250.

Evans, J.E., and D. Turnbull, 1985: The FAA/MIT Lincoln Laboratory Doppler Weather Radar Program. Preprints, 2nd International Conference on the Aviation Weather System. Montreal, Canada, American Meteorological Society, pp. 76–79.

Fujita, T.T., 1980: Downbursts and Microbursts – An Aviation Hazard. Preprints, 11th Conference on Radar Meteorology, Miami Beach, American Meteorological Society, pp. 94–101.

Fujita, T.T., 1985: The Downburst – Microburst and Macroburst. University of Chicago, 122 pp.

Merritt, M.W., 1987: Automated Detection of Microburst Windshear for Terminal Doppler Weather Radar. Preprints, Digital Image Processing and Visual Communications Technologies in Meteorology, Cambridge, MA, SPIE.

National Research Council, 1983: Low–Altitude Wind Shear and its Hazard to Aviation. National Academy Press, 112 pp.

Pike, J.M., F.V. Brock, and S.R. Semmer, 1983: Integrated Sensors for PAM II. Proceedings of the Fifth Symposium on Meteorological Observations and Instrumentation, Toronto, Ontario, Canada.

Rinehart, R.E., J.T. DiStefano, and M.M. Wolfson, 1986: Preliminary Memphis FAA Lincoln Laboratory Operational Weather Studies Results. MIT, Lincoln Laboratory Project Report ATC–141.

Wilson, J.W., R.D. Roberts, C. Kessinger, and J. McCarthy, 1984: Microburst Wind Structure and Evaluation of Doppler Radar for Airport Wind Shear Detection. Journal of Climate and Applied Meteorology, **23**, 895–915.

Wolfson, M.M., J.T. DiStefano, and B.E. Forman, 1986: The FLOWS Automatic Weather Station Network in Operation. MIT, Lincoln Laboratory Project Report ATC–134, FAA Report DOT/FAA/PM–85–27, 284 pp.